Lifetime Evolution of Outer Tropical Cyclone Size and Structure as Diagnosed from Reanalysis and Climate Model Data

BENJAMIN A. SCHENKEL,[a,b] NING LIN,[a] DANIEL CHAVAS,[c] GABRIEL A. VECCHI,[d,e] MICHAEL OPPENHEIMER,[f] AND ALAN BRAMMER[g]

[a] *Department of Civil and Environmental Engineering, Princeton University, Princeton, New Jersey*
[b] *Cooperative Institute for Mesoscale Meteorological Studies, and School of Meteorology, University of Oklahoma, Norman, Oklahoma*
[c] *Department of Earth, Atmospheric, and Planetary Sciences, Purdue University, West Lafayette, Indiana*
[d] *Department of Geosciences, and Princeton Environmental Institute, Princeton University, Princeton, New Jersey*
[e] *NOAA/Geophysical Fluid Dynamics Laboratory, Princeton, New Jersey*
[f] *Woodrow Wilson School of Public and International Affairs, and Department of Geosciences, Princeton University, Princeton, New Jersey*
[g] *Department of Atmospheric and Environmental Science, University at Albany, State University of New York, Albany, New York*

(Manuscript received 21 September 2017, in final form 6 July 2018)

ABSTRACT

The present study examines the lifetime evolution of outer tropical cyclone (TC) size and structure in the North Atlantic (NA) and western North Pacific (WNP). The metric for outer TC size is the radius at which the azimuthal-mean 10-m azimuthal wind equals $8\,\mathrm{m\,s^{-1}}$ (r_8) derived from the NCEP Climate Forecast System Reanalysis (CFSR) and GFDL High-Resolution Forecast-Oriented Low Ocean Resolution model (HiFLOR). Radial profiles of the azimuthal-mean 10-m azimuthal wind are also analyzed to demonstrate that the results are robust across a broad range of wind radii. The analysis shows that most TCs in both basins are characterized by 1) minimum lifetime r_8 at genesis, 2) subsequent substantial increases in r_8 as the TC wind field expands, 3) peak r_8 values occurring near or after the midpoint of the TC lifetime, and 4) nontrivial decreases in r_8 and outer winds during the latter part of the TC lifetime. Compared to the NA, WNP TCs are systematically larger up until the end of their lifetime, exhibit r_8 growth and decay rates that are larger in magnitude, and are characterized by an earlier onset of lifetime maximum r_8 near their lifetime midpoint. In both basins, the TCs exhibiting the largest r_8 increases are the longest lived, especially those that traverse the longest distances (i.e., recurving TCs). Finally, analysis of TCs undergoing extratropical transition (ET) shows that NA TCs exhibit negligible changes in r_8 during ET, while WNP ET cases either show r_8 decreases (CFSR) or negligible changes in r_8 (HiFLOR).

1. Introduction

The size of the tropical cyclone (TC) wind field has been used to describe the dimensions of both the inner and outer near-surface wind field (e.g., Brand and Guard 1979; Liu and Chan 1999; Kimball and Mulekar 2004). Despite the similar terminology, discriminating between outer and inner TC size is crucial given their differing variability resulting from differences in their physics and dynamics (e.g., Emanuel 2004; Smith et al. 2009; Chavas et al. 2015). Specifically, inner TC size encompasses the strongest winds and convection near the TC center, which can be approximately characterized as an air–sea flux–driven heat engine modified by the deleterious impacts of environmental vertical wind shear and dry air (e.g., Emanuel 1986; Tang and Emanuel 2010; Lin et al. 2017). In contrast, outer TC size is measured at radii where convection is minimal, and the atmosphere is approximately in radiative–subsidence balance (Emanuel 2004; Chavas et al. 2015; Chavas and Lin 2016). However,

---

Denotes content that is immediately available upon publication as open access.

Supplemental information related to this paper is available at the Journals Online website: https://doi.org/10.1175/JCLI-D-17-0630.s1.

Corresponding author: Benjamin A. Schenkel, benschenkel@gmail.com

DOI: 10.1175/JCLI-D-17-0630.1

our understanding of the variability of outer size and the factors that control it remains limited. The present study examines the lifetime evolution of outer TC size and structure for North Atlantic (NA) and western North Pacific (WNP) TCs using data from the National Centers for Environmental Prediction (NCEP) Climate Forecast System Reanalysis (CFSR; Saha et al. 2010) and Geophysical Fluid Dynamics Laboratory (GFDL) High-Resolution Forecast-Oriented Low Ocean Resolution model (HiFLOR; Murakami et al. 2015).

Despite several recent studies of outer size, our current understanding of its lifetime evolution remains uncertain. Specifically, prior work has noted substantial interbasin and intrabasin variability in outer TC size (e.g., Merrill 1984; Chavas and Emanuel 2010; Chan and Chan 2015). These differences in outer size may begin at genesis, with genesis outer size hypothesized to be set by both the outer size of the TC-precursor disturbance (e.g., Rotunno and Emanuel 1987; Cocks and Gray 2002; Lee et al. 2010) and the TC genesis environment (e.g., environmental angular momentum; Merrill 1984; Chan and Chan 2012, 2013). However, there have been no prior observational studies of genesis outer size or the factors that may influence it. Moreover, prior work has suggested that most TCs exhibit increases in outer TC size following genesis, but there are inconsistencies in their conclusions ranging between small increases confined to the first two days of the TC lifetime to near-constant, large increases throughout the TC lifetime (e.g., Merrill 1984; Cocks and Gray 2002; Chavas and Emanuel 2010; Knaff et al. 2014). Near the end of the TC lifetime, prior work has suggested that outer size may exhibit a variety of different changes likely dependent on the storm environment (e.g., environmental baroclinicity; Cocks and Gray 2002; Kimball and Mulekar 2004; Kimball 2006), although there has yet to be a study specifically focused on outer size evolution during the end of the TC lifetime. Even during extratropical transition (ET) or, more generally, TCs that encounter baroclinic environments, prior studies have noted increases in outer size, albeit with substantial interstorm variability that has not been well constrained (Brand and Guard 1979; Hart et al. 2006; Evans and Hart 2008; Maclay et al. 2008). Moreover, many of these prior ET studies have been exclusively confined to the NA and utilized small sample sizes, limiting the broader applicability of their results (e.g., Brand and Guard 1979; Hart et al. 2006).

The uncertainties in the lifetime evolution of outer TC size arise from several factors, including 1) the absence of a consistent outer size metric used among studies, which makes it challenging to intercompare results; 2) the use of limited sample sizes; 3) a focus upon specific TC subsets; and most importantly, 4) the shortage of observational studies focused on the lifetime evolution of outer TC size (Merrill 1984; Cocks and Gray 2002). The lack of observational studies is due to the inability of observational datasets to homogenously sample the TC wind field or uniformly sample outer TC size throughout the storm lifetime for a large quantity of storms (e.g., ~30% of TCs sampled by scatterometers; Brand and Guard 1979; Liu and Chan 1999; Chan and Chan 2012). Moreover, several of the previously used datasets are derived partially from subjective analyses, which may introduce a priori biases in outer TC size estimates (e.g., Brand and Guard 1979; Merrill 1984; Kimball and Mulekar 2004). Given these uncertainties, there is a need for an analysis that utilizes a relatively large, observationally constrained, objective dataset to investigate the lifetime evolution of outer TC size and structure.

The present study utilizes an outer size dataset derived from a reanalysis (NCEP CFSR) for all observed TCs, which has been shown to strongly agree with observationally based outer TC size data (Schenkel et al. 2017). The advantages of this CFSR-derived outer TC size dataset compared to earlier studies include 1) spatiotemporal homogeneity in data coverage over the entire TC wind field for observed TCs, 2) consistent representation of TCs in time because of the use of a fixed global numerical weather prediction model and data assimilation system that assimilates historical observations (Thorne and Vose 2010; Bosilovich et al. 2013; Parker 2016), and 3) availability of at least 30 years of data with 6-h temporal resolution. We complement our CFSR dataset with one derived from a high-resolution current-climate model simulation (GFDL HiFLOR) containing a realistic representation of TC frequency, intensity, and structure (Murakami et al. 2015, 2016). Specific complementary advantages of HiFLOR over the CFSR include 1) a larger TC sample size (i.e., 55% more years of data), 2) the absence of potential spurious behavior in reanalyses introduced by spatiotemporal changes in the observing system (e.g., Manning and Hart 2007; Thorne and Vose 2010; Parker 2016), and 3) finer grid spacing (i.e., HiFLOR horizontal grid spacing is half of CFSR).

The HiFLOR simulation also has its deficiencies, namely, the absence of a strong observational constraint on TC activity and the large-scale atmosphere resulting in nontrivial biases in TC intensity, frequency, and track (e.g., Murakami et al. 2015). However, it is unclear how, if at all, these biases feed back onto the HiFLOR outer TC size distribution. Specifically, the biases in HiFLOR TC intensity likely do not impact outer TC size given that the two do not vary strongly with one another (e.g., Merrill 1984; Chavas and Emanuel 2010; Chavas et al.

2016). Moreover, while outer size does vary with both TC latitude and longitude (e.g., Merrill 1984; Chavas and Emanuel 2010; Chan and Chan 2015), it is unclear which physical mechanisms govern these spatial variations and, hence, how TC track biases may impact the distribution of the outer wind field structure and size in HiFLOR. In contrast to HiFLOR, the strong observational constraint imposed by the data assimilation system of the CFSR provides a complementary benefit over this weakness of HiFLOR (Saha et al. 2010). Despite the absence of assimilated observations, HiFLOR can provide a reasonable representation of TC structure for the present climate (e.g., Murakami et al. 2015, 2016). Together, agreement between these datasets provides substantially greater confidence in our analysis compared to analyzing these datasets in isolation from one another given their respective biases.

Leveraging the large sample sizes from the NCEP CFSR reanalysis and the GFDL HiFLOR simulation, the present study provides a statistical examination of the lifetime evolution of outer TC size and wind structure in the NA and WNP. Considering the uncertainties in prior work, this study will address the following questions:

- How does outer TC size at genesis compare to that during the rest of the TC lifetime?
- How does outer TC size evolve to its peak, and how does it change thereafter?
- How does outer TC size evolve during ET?
- Is the lifetime evolution of outer size different between NA and WNP TCs?

This study will address these questions by examining outer TC size and structure during three lifetime milestones to facilitate intercomparing TCs with different lifetime durations (Cocks and Gray 2002; Chan and Chan 2012): 1) genesis, 2) time of lifetime maximum outer size, and 3) end of TC lifetime. This work provides the foundation for follow-up statistical modeling of the evolution of outer size and analysis of potentially influential environmental variables. The remainder of this manuscript is divided into three parts. Section 2 describes the data and methods used, section 3 presents the results, and section 4 provides a discussion and conclusion.

2. Data and methods

a. Best track TC data

Best track data are employed to locate TCs in the CFSR. The present study examines NA and WNP TCs from 1979 to 2010 in version 3, revision 9, of the International Best Track Archive for Climate Stewardship (IBTrACS; Knapp et al. 2010). National Hurricane Center data are used for NA TCs, while Joint Typhoon Warning Center data are used for WNP TCs. NA and WNP TCs are chosen based on prior work demonstrating that reanalysis TC intensity, track, and outer TC structure are sufficiently well represented in these two basins (e.g., Schenkel and Hart 2012; Murakami 2014; Hodges et al. 2017; Schenkel et al. 2017) and to avoid the greater uncertainty of IBTrACS data in other TC basins (e.g., Landsea et al. 2006).

Only those storms with a maximum azimuthal-mean 10-m azimuthal wind v^*_{max} greater than or equal to $15\,\mathrm{m\,s^{-1}}$ are examined, with v^*_{max} defined as (Chavas and Lin 2016)

$$v^*_{\mathrm{max}} = 0.8(V_{\mathrm{max,IB}} - 0.55V_{\mathrm{trans,IB}}), \quad (1)$$

where $V_{\mathrm{max,IB}}$ is the IBTrACS maximum 10-m wind speed, and $V_{\mathrm{trans,IB}}$ is the IBTrACS TC translation speed. The variable v^*_{max} is used instead of $V_{\mathrm{max,IB}}$ for two reasons: 1) to exclude weak TCs embedded in strong environmental steering flows and 2) because of its greater relevance to existing TC intensity theory (Chavas and Lin 2016; Chavas et al. 2016). The analysis also excludes all 6-h IBTrACS data in which the TC is over land.

b. TC wind field datasets

To provide multidecadal estimates of outer TC size and structure, data are derived from both the NCEP CFSR and GFDL HiFLOR. Table 1 provides salient details for both the CFSR and HiFLOR. The CFSR provides outer TC size and wind field data for IBTrACS TCs. The CFSR is a 0.5° × 0.5° 6-h, 32-yr (1979–2010) reanalysis dataset (Saha et al. 2010). It is chosen because of its better representation of IBTrACS TC position and intensity (Schenkel and Hart 2012; Murakami 2014; Hodges et al. 2017; Schenkel et al. 2017) and of observed outer TC size and structure, despite the underestimation of inner-core winds (i.e., radius < 300 km; Schenkel et al. 2017). Given that nontrivial position differences occasionally arise between IBTrACS and the CFSR (e.g., Schenkel and Hart 2012; Murakami 2014; Hodges et al. 2017), the 6-h location of each reanalysis TC is determined by using the IBTrACS location as a first guess before determining the final reanalysis TC location. The final TC location is calculated using the mean of the centers of mass for six different variables: mean sea level pressure; 925-, 850-, and 700-hPa relative vorticity; and 850- and 700-hPa geopotential height (e.g., Marchok 2002; Brammer 2017; Schenkel et al. 2017). CFSR TC genesis is defined, using IBTrACS data, as the first 6-h point at which $v^*_{\mathrm{max}} \geq 15\,\mathrm{m\,s^{-1}}$, while being subjectively classified as a TC in IBTrACS.

TABLE 1. Native grid spacing, postprocessed grid spacing, grid spacing of radial profile of TC winds in this study, period of data availability, supplemental initialization of TCs, and the reference for each dataset. For the number denoting the native grid spacing, T refers to the mean wave truncation number, C refers to the number of points across each model tile for a cubed sphere grid, and L refers to the number of vertical levels.

Dataset	Native grid spacing	Postprocessed grid spacing	Radial profile grid spacing	Period	TC initialization	Reference
NCEP CFSR	T382, L64	0.50° × 0.50°, L37	27.5 km	1979–2010	Vortex relocation	Saha et al. (2010)
GFDL HiFLOR	C360, L32	~25 km × ~25 km, L4	12.5 km	50-yr current-climate simulation	None	Murakami et al. (2015)

Outer TC size data are also obtained from the HiFLOR model, which provides 50 years of 6-h data on a ~25 km × ~25 km grid (Murakami et al. 2015). HiFLOR is a coupled climate model forced with 1995 radiative forcing conditions and sea surface temperatures (SSTs) nudged on a 5-day restoring time scale toward a monthly varying climatological SST derived from the Met Office Hadley Centre SSTs averaged between 1986 and 2005 (Rayner et al. 2003). HiFLOR represents one of the first climate model simulations with realistic TC frequency, intensity, and structure (Murakami et al. 2015, 2016). HiFLOR does not replicate any specific historical TC but rather provides dynamically consistent realizations of TC activity given current-climate conditions. HiFLOR TCs are tracked using a combination of closed mean sea level pressure contours and upper-tropospheric temperature anomalies (Murakami et al. 2015; Harris et al. 2016; Murakami et al. 2016). Like Murakami et al. (2015), TC genesis in HiFLOR is defined as the start time of at least 24 consecutive hours of the TC attaining both an upper-tropospheric warm core and $v^*_{\max} \geq 15\,\mathrm{m\,s^{-1}}$.

c. Outer TC size metric

The outer TC size metric utilized in this study is the radius at which the azimuthal-mean 10-m azimuthal wind equals $8\,\mathrm{m\,s^{-1}}$ (r_8). In addition to being similar to previously used outer TC size metrics (Chavas and Emanuel 2010; Chavas et al. 2016, 2017), r_8 is chosen because it is represented with the greatest fidelity in the CFSR compared to observations (Schenkel et al. 2017). The results for r_8 are applicable across a variety of outer size metrics [e.g., radius of azimuthal-mean near-surface azimuthal wind equals $17\,\mathrm{m\,s^{-1}}$ (r_{17})] as shown in a supplemental figure constructed using r_{17} from HiFLOR (Fig. S1 in the online supplemental material) and implied in radial profiles of azimuthal wind shown later. The term r_8 is derived from both the CFSR and HiFLOR as follows (Chavas and Vigh 2014; Schenkel et al. 2017): 1) 10-m total wind vectors are interpolated to a TC-centered polar coordinate system; 2) the environmental wind is removed from the total wind field, with the environmental wind empirically estimated as the TC translation vector rotated 20° cyclonically and reduced by a factor of 0.55 (Lin and Chavas 2012); 3) the azimuthal-mean azimuthal wind field is computed excluding land grid points; 4) the azimuthal-mean azimuthal wind is interpolated to a uniformly spaced radial grid with a resolution that is 0.5 times the horizontal grid spacing of the input data; and 5) r_8 is extracted from the radial profile only for TCs that have missing data radially inwards of r_8 over the equivalent of two consecutive CFSR grid points (i.e., ~100 km) or less (Schenkel et al. 2017). The present study focuses on examining those TCs in which r_8 is consistently defined throughout the TC lifetime, with the corresponding sample sizes provided in Table 2.

d. ET definition

The start and end time of ET in the present study is defined using the cyclone phase space (Hart 2003), which is computed from CFSR and HiFLOR data. In the cyclone phase space, ET start is defined as when the lower-tropospheric thermal asymmetry parameter B exceeds an empirically defined value of 10 m, indicative that the TC has acquired a frontal structure (i.e., warm, moist air located to the east and cold, dry air located to the west of a poleward-moving TC), while the lower-tropospheric thermal wind parameter $-V_L^T$ exceeds 0, suggestive of a cyclone with a lower-tropospheric warm core (i.e., geostrophic wind speed decreasing with height associated with a warm, moist lower troposphere). The end of ET occurs when the lower-tropospheric warm core finally transitions to a cold core ($-V_L^T < 0$; i.e., geostrophic wind speed increasing with height associated with a cold, dry lower troposphere; Hart 2003; Evans and Hart 2003; Kitabatake 2011). The cyclone phase parameters in the CFSR are calculated from data at 50-hPa intervals from 900 to 600 hPa, while HiFLOR computations use only available data at 850 and 500 hPa, which may yield slightly earlier ET start and end times (Liu et al. 2017).

The present study also employs two additional criteria when defining ET. First, the TC must continuously maintain a warm core for two days prior to ET start or from genesis to ET start for TCs with lifetimes shorter

TABLE 2. Sample size of all TCs and ET cases examined in the present study within the CFSR and HiFLOR for NA and WNP TCs.

Dataset and basin	All TCs	ET TCs
NA CFSR	144	41
WNP CFSR	416	60
NA HiFLOR	336	119
WNP HiFLOR	1690	541

than two days to remove storms with underresolved structure (e.g., Evans and Hart 2003; Manning and Hart 2007; Wood and Ritchie 2014). Second, reanalysis TCs that attain a lower-tropospheric cold core prior to or upon attaining frontal structure ($B > 10$) are not considered here, since this structural evolution is due to underresolved reanalysis TC structure rather than ET processes (e.g., Evans and Hart 2003; Kitabatake 2011; Wood and Ritchie 2014). These two criteria together with the exclusion of overland cases and the inclusion of only those cases where r_8 is continuously defined reduces the number of ET cases, which are given in Table 2. While our use of an axisymmetric framework for studying changes in the outer TC wind structure does not account for the development of wind field asymmetries during ET, prior work has shown that these asymmetries only begin to strongly manifest themselves at or after the completion of ET (e.g., Evans and Hart 2008; Loridan et al. 2014, 2015), suggesting that our axisymmetric framework is suitable for studying ET cases.

e. Statistical significance methodology

All statements made in the results are supported by statistical significance testing, although the specific p values and testing methodologies are not explicitly provided for each result. Specifically, Pearson correlation coefficients are stated if they are statistically significantly different from 0 at the 95% confidence interval according to a Fischer transformation. Two distributions are discussed as being statistically significantly different from one another if both of the following conditions are met: 1) two distributions originated from different parent distributions as diagnosed by a two-sample Kolmogorov–Smirnov test at the 5% level and 2) median values are statistically significantly different according to a 1000-sample bootstrap approach with replacement for a two-tailed test at the 95% confidence interval. For each statistical significance test, the number of uniquely named TCs, rather than the number of 6-h IBTrACS data points, is conservatively used as the number of degrees of freedom, which provides a stricter testing criterion.

3. Results

The analysis begins by examining case studies followed by the composited lifetime evolution of r_8 for NA and WNP TCs. Following this, the interstorm variability in r_8, its rate of change, and outer TC structure are analyzed at genesis, the onset of lifetime maximum r_8, and the end of lifetime. The final results section examines r_8 changes during ET. The composited lifetime evolution (Fig. 2) has also been recreated for r_{17} from HiFLOR and is provided as supplemental material (Fig. S1) to demonstrate that these results extend beyond a single outer size metric. All salient relationships are quantified via Pearson correlation coefficients, which are centrally located in Table 3.

a. Overview of lifetime evolution of outer TC size

Representative case studies of the lifetime evolution of r_8 are provided for the CFSR and HiFLOR in the NA (Fig. 1a) and WNP (Fig. 1b). The NA cases in both the CFSR and HiFLOR (Fig. 1a) exhibit growth in r_8 during most of their lifetimes, exhibiting peak values that are over 50% larger than their genesis r_8. In contrast, WNP cases in both the CFSR and HiFLOR (Fig. 1b) initially grow more rapidly, with peak values occurring earlier (i.e., near the TC lifetime midpoint) before undergoing large decreases in r_8. The WNP HiFLOR case serves as an example of the nontrivial fraction of TCs that exhibit their largest growth in r_8 during the first several days of their lifetime, similar to prior work (Chavas and Emanuel 2010; Smith et al. 2011; Chavas and Lin 2016).

The composited lifetime evolution of r_8 from the CFSR and HiFLOR is plotted in normalized coordinates and binned according to normalized age for TCs with short, normal, and long lifetimes in the NA (Figs. 2a,b) and WNP (Figs. 2c,d). Similar to the representative case studies, NA TCs with normal and long lifetimes grow throughout their life cycles and reach peak values near the end of their lifetimes in the CFSR and HiFLOR, similar to prior analyses of NA storms (e.g., Merrill 1984; Kossin et al. 2007; Knaff et al. 2014). Peak median r_8 in the NA ranges between 1.25 and 1.49 times its first quartile r_8 in the CFSR and between 1.45 and 1.65 times the first quartile r_8 in HiFLOR. In the WNP, TCs with normal and long lifetimes in the CFSR and HiFLOR grow at a faster normalized rate compared to the NA primarily during the first half of their lifetimes, reaching peak r_8 around the midpoint of their lifetimes and decreasing thereafter. Peak median r_8 for WNP TCs is smaller in normalized magnitude in the CFSR (1.15–1.33 times the first quartile r_8) and HiFLOR (1.30–1.46 times the first quartile r_8) relative to the NA. The midpoint lifetime peak in r_8 contrasts with the near-constant increase

TABLE 3. Summary table of Pearson correlation coefficients between various quantities mentioned throughout the text [corr(X, Y)] for CFSR and HiFLOR data in the NA and WNP. All correlations are statistically significantly different from zero at the 95% confidence interval.

X	Y	NA CFSR	NA HiFLOR	WNP CFSR	WNP HiFLOR
r_8	TC age	0.30	0.39	0.17	0.23
Genesis r_8	Lifetime max r_8	0.66	0.48	0.60	0.49
Timing of lifetime max r_8	Lifetime max r_8 − genesis r_8	0.74	0.58	0.65	0.59
Meridional distance traveled up to lifetime max r_8	Lifetime max r_8 − genesis r_8	0.67	0.70	0.53	0.45
Zonal distance traveled up to lifetime max r_8	Lifetime max r_8 − genesis r_8	0.62	0.59	0.56	0.49
TC lifetime	Lifetime max r_8 − genesis r_8	0.56	0.44	0.54	0.52
End-of-lifetime latitude − genesis latitude	Lifetime max r_8 − genesis r_8	0.54	0.58	0.39	0.31
Lifetime max r_8	End-of-lifetime r_8	0.78	0.82	0.69	0.75
Lifetime max r_8	End-of-lifetime r_8 − genesis r_8	−0.53	−0.52	−0.54	−0.48
Genesis r_8	End-of-lifetime r_8	0.28	0.31	0.33	0.29
Timing of end of lifetime − timing of lifetime max r_8	End-of-lifetime r_8 − lifetime max r_8	−0.44	−0.29	−0.38	−0.50

in WNP outer TC size shown by Cocks and Gray (2002), which employed subjectively derived outer size estimates. Finally, short-lived TCs in both basins exhibit marginal or even negligible changes in r_8 during their lifetimes.

These results suggest that most NA TCs exhibit growth in r_8 throughout much of their lifetimes, while the majority of WNP TCs exhibit growth until a midpoint lifetime peak followed by substantial decreases. The interbasin and intrabasin differences in the lifetime evolution of r_8 may suggest the importance of the TC environment (e.g., Merrill 1984; Liu and Chan 1999; Chan and Chan 2012, 2013). Alternatively, internal dynamical factors cannot be ruled out given that the increases in r_8 coincide with TC intensification (not shown), especially during the 1–2 days following genesis (e.g., Chavas and Emanuel 2010; Knaff et al. 2014; Chavas and Lin 2016). For WNP TCs, the midlifetime maximum in r_8 appears consistent with a subtropical peak attributed to the interaction between increasing vortex inertial stability and increasing environmental angular momentum (e.g., Smith et al. 2011; Chan and Chan 2013, 2014). Moreover, the interbasin differences in r_8 evolution may be explained by stronger, lower-latitude meridional gradients of the environmental thermodynamic variables relevant to r_8 in the WNP (e.g., relative humidity, potential intensity; Emanuel 1986; Kimball 2006; Hill and Lackmann 2009; Chavas and Emanuel 2014). Finally, these results suggest that TC age (i.e., time since genesis) is not a strong proxy for the factors that control outer size, in contrast to Kossin et al. (2007), as supported by negligible (WNP) to weakly (NA) positive correlations in both the CFSR and HiFLOR (Table 3).

b. *Outer TC size evolution from genesis to maximum value*

1) CHANGES IN r_8 FROM GENESIS TO LIFETIME MAXIMUM VALUE

The present section focuses on the interstorm variability in r_8 evolution between genesis and lifetime maximum r_8 by examining joint histograms of these two quantities from CFSR and HiFLOR TCs in the NA (Figs. 3a,b) and WNP (Figs. 3c,d). Both the variability

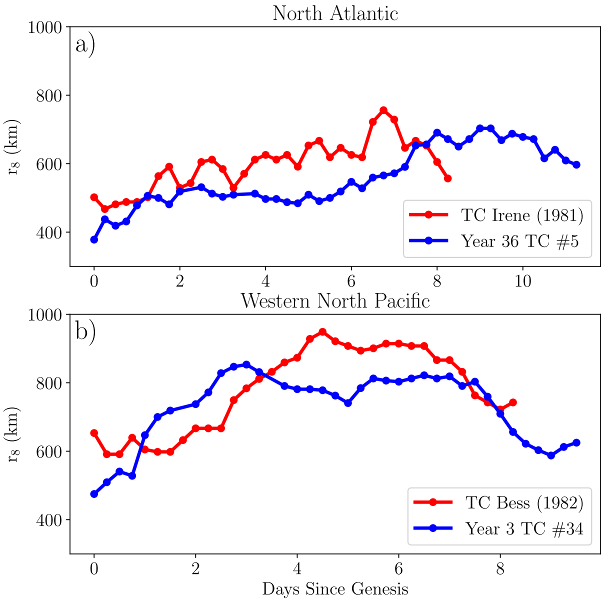

FIG. 1. Time series of r_8 (km) for representative case studies including (a) NA TC Irene (1981) in the CFSR and TC 5 from year 36 in the HiFLOR simulation and (b) WNP TC Bess (1982) in the CFSR and TC 34 from year 3 of the HiFLOR simulation.

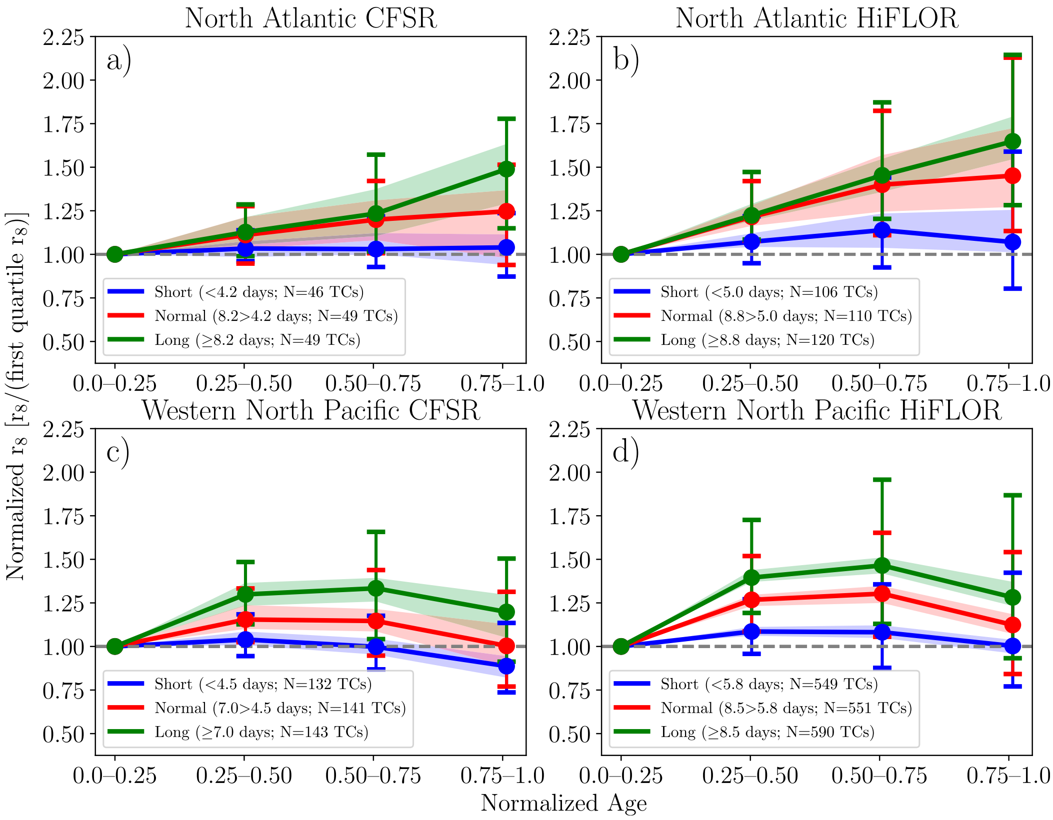

FIG. 2. Composited time series of the median (solid line) with its 95% confidence interval calculated from a 1000-sample bootstrap approach with replacement (shading) and the interquartile range (error bars) of normalized r_8 [r_8/(first quartile r_8)] binned according to normalized age for TCs with short, normal, and long lifetimes for (a) NA CFSR, (b) NA HiFLOR, (c) WNP CFSR, and (d) WNP HiFLOR TCs. Normalized age is used as the time coordinate split into quartiles, with r_8 values binned and averaged within each quartile for a given TC. The r_8 values in each quartile are normalized by dividing by the first quartile r_8. TCs are subdivided into cases with short, normal, and long lifetimes corresponding to the first, second, and third tercile of TC lifetime, respectively.

and magnitude of lifetime maximum r_8 are larger than at genesis, with median r_8 increasing by 60% in both basins within the CFSR and HiFLOR. Such a result agrees with the higher end of r_8 growth estimates from prior work (e.g., Merrill 1984; Cocks and Gray 2002; Chan and Chan 2014). Moderate positive correlations exist between genesis and lifetime maximum r_8 (Table 3) in the NA and WNP, suggesting that genesis r_8 imparts some memory into the later stages of the TC lifetime, similar to prior work (e.g., Rotunno and Emanuel 1987; Cocks and Gray 2002; Lee et al. 2010). With regards to interbasin differences, WNP r_8 is larger and exhibits greater variability during both genesis and lifetime maximum r_8 (Figs. 3c,d) compared to the NA (Figs. 3a,b), suggesting that the previously observed interbasin differences (e.g., Merrill 1984; Liu and Chan 1999; Chavas and Emanuel 2010; Chan and Chan 2015) begin at genesis. In particular, median genesis r_8 for WNP TCs is ~35% larger in both the CFSR and HiFLOR compared to NA TCs, with similar differences found at lifetime maximum r_8.

Radial profiles of the azimuthal-mean 10-m azimuthal winds in a normalized radial coordinate system are also presented for NA (Figs. 4a,b) and WNP TCs (Figs. 4c,d) in the CFSR and HiFLOR during genesis and lifetime maximum r_8. The wind speed is consistently greater at all radii for lifetime maximum r_8 compared to genesis r_8.

The results presented here suggest that the outer TC wind field broadens over time for most TCs in the NA and WNP. Moreover, the previously documented larger outer size of WNP TCs relative to the NA begins at genesis. The broader genesis r_8 distribution in the WNP may be reflective of the greater variety of WNP TC-precursor disturbances with differing horizontal length scales (e.g., monsoon gyre, mixed Rossby–gravity waves; Lander 1994; Dickinson and Molinari 2002; Frank and Roundy 2006) that are comparable or larger than NA precursor disturbances (e.g., easterly waves; Burpee 1974; Reed et al. 1977; Diaz and Aiyyer 2013). The expansion of r_8 following

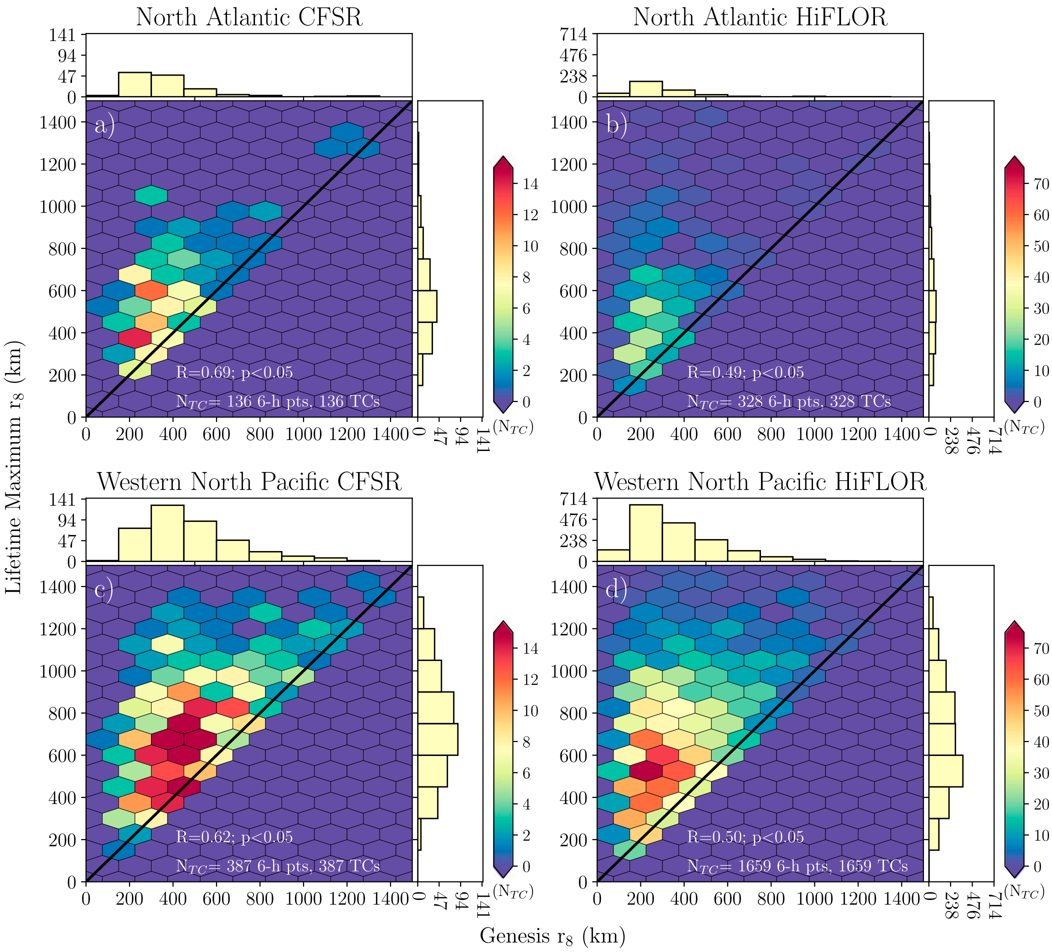

FIG. 3. Joint histogram (shaded hexagons) of genesis r_8 (km) vs lifetime maximum r_8 (km) for (a) NA CFSR, (b) NA HiFLOR, (c) WNP CFSR, and (d) WNP HiFLOR TCs. The black solid line denotes the 1:1 line between genesis r_8 and lifetime maximum r_8. The one-dimensional histograms above and to the right of each joint histogram are for the distributions of genesis r_8 and lifetime maximum r_8, respectively. Pearson correlations are provided. Note the color bars and axes ranges are larger for the HiFLOR plots compared to the CFSR.

genesis may be a response to TC translation into dynamic and thermodynamic environments supportive of larger r_8, especially given the large quantities of angular momentum necessitated to support the expansion of the TC wind field (e.g., Merrill 1984; Smith et al. 2011; Chan and Chan 2013). Alternatively, r_8 expansion may be related to the spinup of the TC wind field following genesis (e.g., Chavas and Emanuel 2010; Smith et al. 2011; Chavas and Lin 2016).

2) TIME SCALES OF OUTER SIZE CHANGES FROM GENESIS TO LIFETIME MAXIMUM VALUE

The time scales of these changes in r_8 are examined using joint histograms of the timing of lifetime maximum r_8 versus the difference between lifetime maximum r_8 and genesis r_8 for NA (Figs. 5a,b) and WNP TCs (Figs. 5c,d). Both basins show that a later onset of lifetime maximum r_8 is associated with larger r_8 increases in the CFSR and HiFLOR, which is also supported by moderate to strong positive correlations (Table 3). WNP TCs exhibit larger r_8 growth rates (median of 59 km day^{-1} in CFSR and 54 km day^{-1} in HiFLOR) compared to the NA (median of 37 km day^{-1} in CFSR and 35 km day^{-1} in HiFLOR), consistent with larger growth for WNP TCs despite their earlier onset of lifetime maximum r_8.

Shorter time-scale variability in r_8 is examined via box-and-whisker plots and kernel density estimates of the 1-day rate of r_8 change (dr_8/dt) for the NA (Figs. 6a, b) and WNP (Figs. 6c,d). The dr_8/dt distribution is approximately normally distributed but skewed toward positive values for NA and WNP TCs, consistent with the overall growth of r_8. Compared to the NA, the WNP exhibits dr_8/dt that is more positive with a broader range.

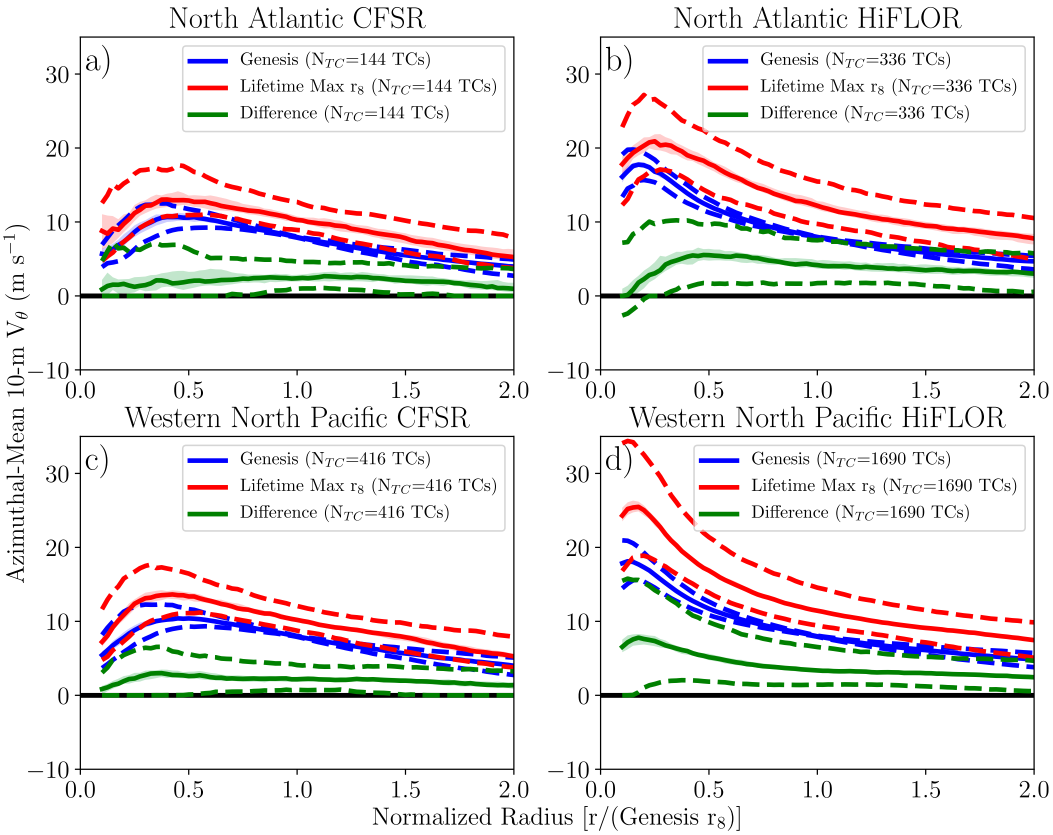

FIG. 4. Radial profile in normalized radial coordinates [r/(genesis r_8)] of the median (solid line) with its 95% confidence interval calculated from a 1000-sample bootstrap approach with replacement (shading) and the interquartile range (dashed lines) for the azimuthal-mean 10-m azimuthal wind (m s^{-1}) at genesis, lifetime maximum r_8, and the difference between the two for (a) NA CFSR, (b) NA HiFLOR, (c) WNP CFSR, and (d) WNP HiFLOR TCs. The distribution of azimuthal winds at each radius during genesis vs lifetime maximum r_8 are statistically significantly different from each other according to two-sample Kolmogorov–Smirnov testing ($p < 0.05$).

These results suggest that WNP TCs grow more rapidly over a shorter period of time than NA TCs. The earlier onset of lifetime maximum r_8 for WNP TCs compared to the NA may be due to their larger genesis r_8 coupled with the greater r_8 growth rate, yielding a quicker approach to the maximum r_8 supported by the environment as suggested by prior work (Chavas and Emanuel 2014; Held and Zhao 2008; Khairoutdinov and Emanuel 2013). The interbasin differences in growth rates and duration of growth may indicate that the salient physical processes may be subjected to differing degrees of forcing in each basin due to differences in the environment (e.g., meridional gradient in environmental relative humidity; Hill and Lackmann 2009; Kimball 2006; Wang 2009).

3) ASSOCIATION OF OUTER SIZE CHANGES WITH TC TRACK ATTRIBUTES

The variability in r_8 evolution between genesis and lifetime maximum r_8 with TC track attributes is examined by comparing the box-and-whisker plots of the zonal (Fig. 7a) and meridional (Fig. 7b) distance traveled prior to lifetime maximum r_8 and timing of lifetime maximum r_8 (Fig. 7c) for TCs that undergo the largest and smallest r_8 changes. TCs exhibiting the largest increases in r_8 traverse both greater zonal and meridional distances prior to lifetime maximum r_8 and exhibit later onsets of lifetime maximum r_8 in the CFSR and HiFLOR within both basins, with all three relationships supported by moderate-to-strong positive correlations (Table 3).

Plan view plots of genesis and track density are shown for the NA (Fig. 8) and WNP (Fig. 9) for TCs that undergo the largest and smallest r_8 changes between genesis and lifetime maximum r_8. WNP TCs that undergo the largest r_8 changes form farther south and east of TCs exhibiting the smallest changes, while no such relationship exists for NA storms. Moreover, the TCs that exhibit the largest r_8 changes are longer lived, traverse a broader latitude band, and cluster into tracks reminiscent of recurving TCs, which is further supported by

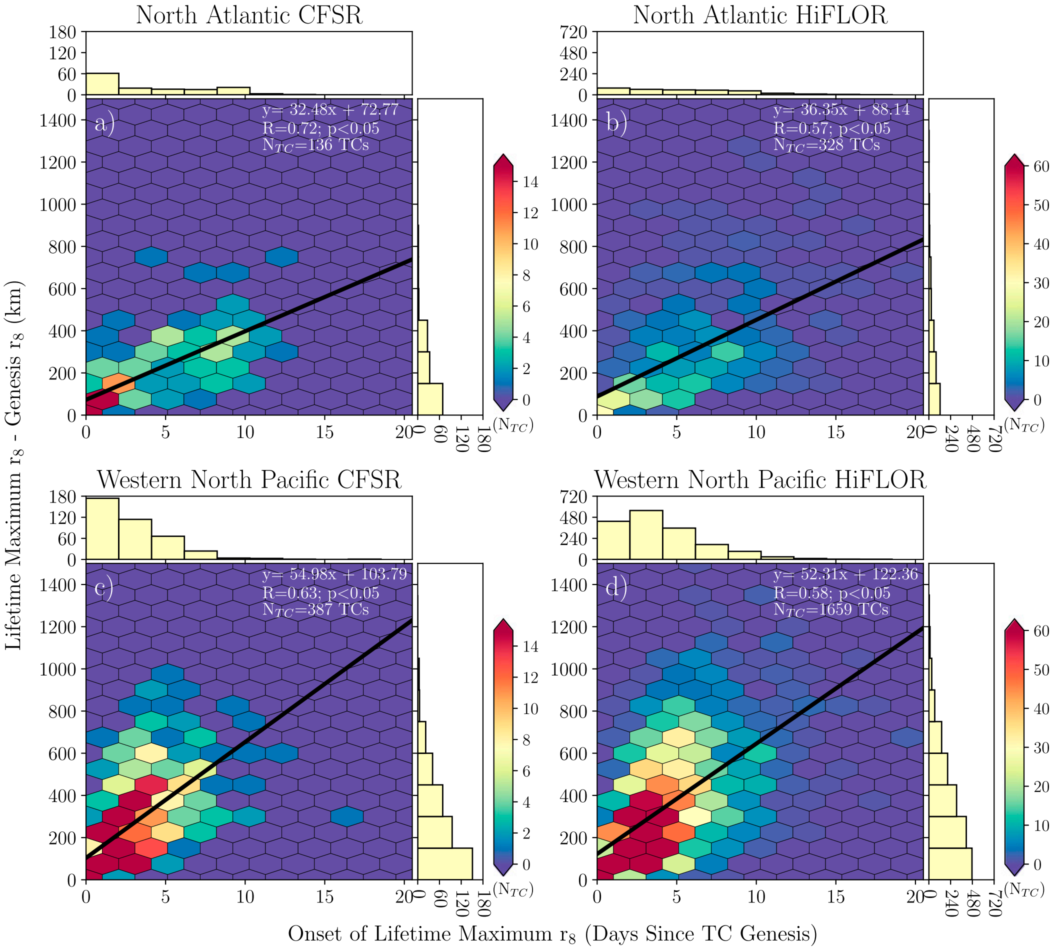

FIG. 5. As in Fig. 3, but for onset of lifetime maximum r_8 (days since genesis) vs difference between lifetime maximum r_8 and genesis r_8 (km). The black solid line denotes the simple linear regression equation between the two quantities with the corresponding equation given in each joint histogram.

both the weak to moderate correlations (Table 3) and prior studies (e.g., Merrill 1984; Lee et al. 2010; Knaff et al. 2014).

These results may suggest that those long-lived TCs with recurving track types are associated with the largest r_8 growth in both basins. Such a result may not be surprising given the slow-varying nature of outer size (e.g., Weatherford and Gray 1988; Merrill 1984; Chavas and Emanuel 2010; Chavas and Lin 2016). Recurving TCs may undergo the largest r_8 increases in response to reaching higher latitudes, which may provide the most favorable environments for outer size changes (e.g., WNP subtropics; Smith et al. 2011; Chan and Chan 2013; Chavas and Emanuel 2014; Chan and Chan 2015). Finally, the tendency for TCs exhibiting the largest r_8 growth to cluster into recurving track types may suggest that the phenomena that influence the TC track and lifetime (e.g., El Niño–Southern Oscillation; Camargo and Sobel 2005; Kossin et al. 2010; Colbert and Soden 2012) may also modulate r_8, perhaps implying some long-term predictability of r_8.

c. *Outer TC size evolution from lifetime maximum to end of lifetime*

1) CHANGES IN r_8 FROM MAXIMUM VALUE TO LIFETIME END

The change in r_8 near the end of the TC lifetime is examined using joint histograms of lifetime maximum r_8 versus the end-of-lifetime r_8 for NA (Figs. 10a,b) and WNP TCs (Figs. 10c,d). Rather than plateauing, r_8 decreases substantially following lifetime maximum r_8 in the CFSR and HiFLOR in both basins. Decreases in median r_8 from lifetime maximum r_8 to the end of the TC lifetime range from 24% in the CFSR and 15% in

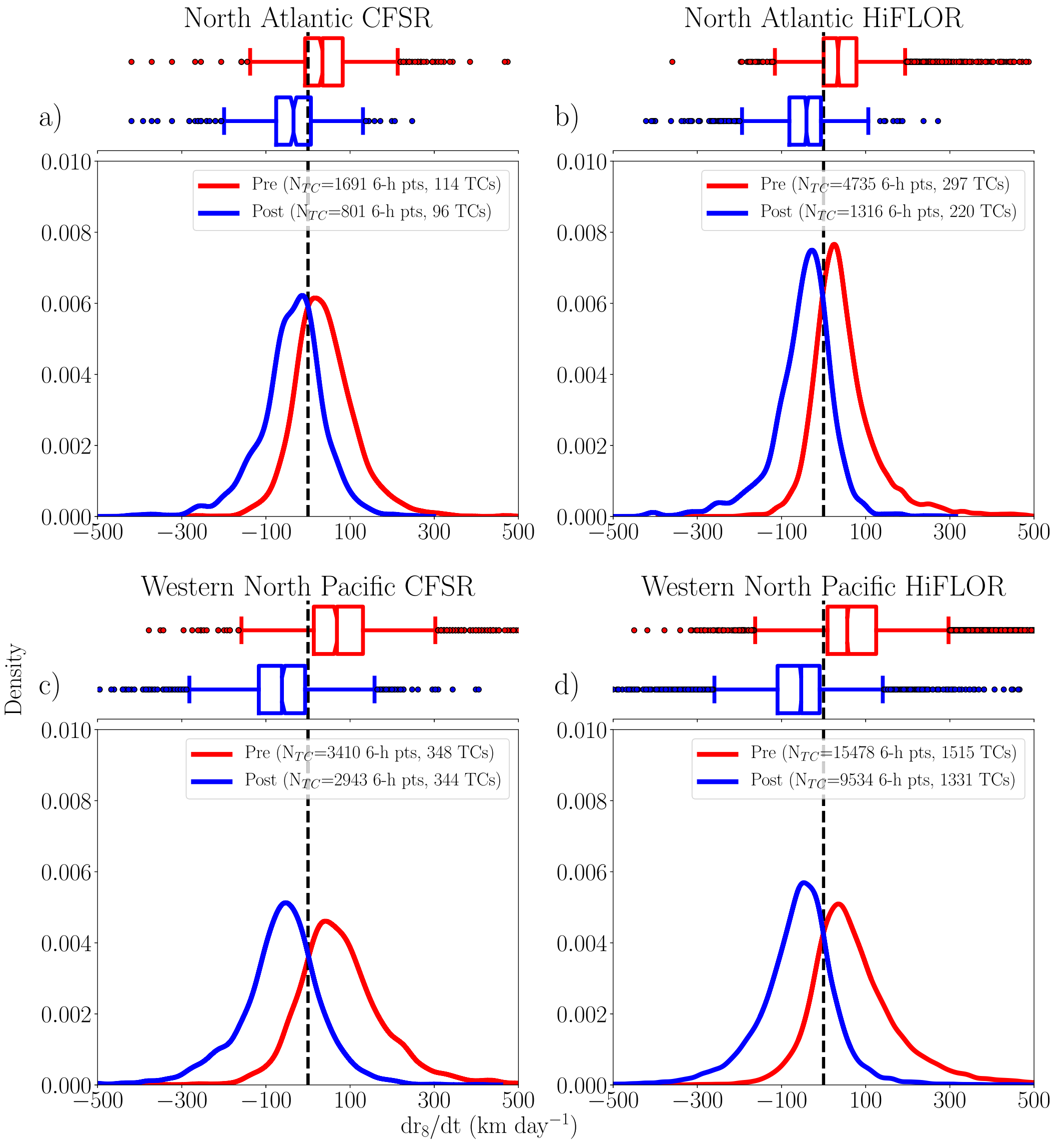

FIG. 6. Kernel density estimate and box-and-whisker plot of daily rate of change in r_8 (dr_8/dt; km day^{-1}) for TCs prior to lifetime maximum r_8 (pre) and after lifetime maximum r_8 (post) in the (a) NA CFSR, (b) NA HiFLOR, (c) WNP CFSR, and (d) WNP HiFLOR. The boxplot displays the median (colored vertical line near the box center), the 95% confidence interval of the median calculated from a 1000-sample bootstrap approach with replacement (colored notches on boxes), the interquartile range [colored box perimeter; (q_1, q_3)], whiskers {colored lines; $[q_1 - 1.5(q_3 - q_1), q_3 + 1.5(q_3 - q_1)]$}, and outliers (colored, filled circles).

HiFLOR for NA TCs to 33% in the CFSR and 34% in HiFLOR for WNP TCs. While agreeing with Knaff et al. (2014; objective size estimates), such a result contrasts with increasing outer size at the end of the TC lifetime for most TCs shown in Cocks and Gray (2002; subjective size estimates). TCs with large lifetime maximum r_8 also remain at the larger end of the r_8 distribution at the end of the TC lifetime (and vice versa) in both datasets within each basin, as shown through moderate-to-strong positive correlations (Table 3). However, larger lifetime maximum r_8 values are also associated with larger decreases in r_8 during the end of the TC lifetime (and vice versa) in both basins, as shown through weak to moderate correlations (Table 3). This relationship is consistent with NA and WNP end-of-lifetime r_8 being comparable despite r_8 being larger for WNP TCs during the earlier stages of the TC lifetime.

To supplement Fig. 10, radial profiles of the azimuthal-mean 10-m azimuthal wind in normalized radial coordinates are shown during lifetime maximum r_8 and

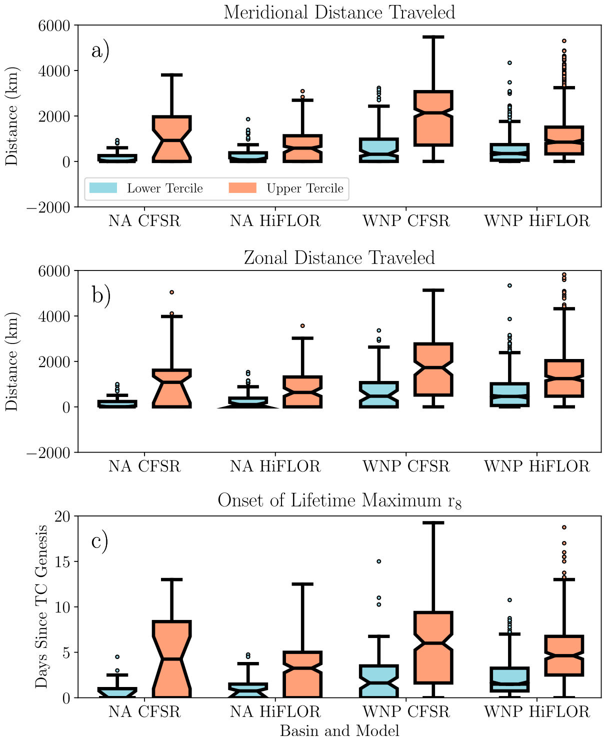

FIG. 7. Box-and-whisker plot of the (a) meridional distance (km) and (b) zonal distance (km) traveled between lifetime maximum r_8 and genesis r_8 and (c) onset of lifetime maximum r_8 (days since TC genesis) for NA CFSR, NA HiFLOR, WNP CFSR, and WNP HiFLOR TCs in the lower and upper tercile of the difference between lifetime maximum r_8 and genesis r_8. The boxplot displays the median (black horizontal line near box center), the 95% confidence interval of the median calculated from a 1000-sample bootstrap approach with replacement (notches on boxes), the interquartile range [box perimeter; (q_1, q_3)], whiskers {black lines; $[q_1 - 1.5(q_3 - q_1), q_3 + 1.5(q_3 - q_1)]$}, and outliers (filled circles).

end-of-lifetime for NA (Figs. 11a,b) and WNP TCs (Figs. 11c,d). In both basins, azimuthal winds decrease during the end of the TC lifetime at outer radii, especially between $0.5 \leq r/(\text{lifetime maximum } r_8) \leq 1.5$, suggestive of a spindown of the entire TC wind field at lifetime end.

Together, these results suggest that TCs in both basins exhibit nontrivial end-of-lifetime decreases in r_8 associated with the weakening of the TC wind field. Assuming poleward movement of the TC, the decrease in r_8 prior to their end of lifetime may be forced by the increasing inertial stability of the vortex and associated reduced efficiency of environmental angular momentum fluxes in changing outer size, which occurs poleward of subtropical latitudes (e.g., Smith et al. 2011; Chan and Chan 2013, 2014). Alternatively, r_8 decreases could be attributed to decreases in relative humidity as TCs move into the subtropics and midlatitudes. Perhaps because of larger TCs exhibiting greater decreases in r_8 at the end of the TC lifetime, genesis r_8 appears to have little bearing upon end-of-lifetime maximum r_8 as shown through weak positive correlations between the two quantities (Table 3), which contrasts with prior work (e.g., Rotunno and Emanuel 1987; Cocks and Gray 2002; Lee et al. 2010).

2) TIME SCALES OF OUTER SIZE CHANGES FROM MAXIMUM VALUE TO END OF LIFETIME

The time scales of the change in r_8 between its maximum value and end of lifetime is shown using joint histograms of r_8 change versus the time of change for NA (Figs. 12a,b) and WNP TCs (Figs. 12c,d). TCs that exist for longer durations following lifetime maximum r_8 undergo larger decreases in r_8, which is also supported by weak to moderate correlations between the two quantities in the CFSR and HiFLOR in both basins (Table 3). During the end of lifetime, the rate of r_8 change is larger for WNP TCs (mean $-37\,\text{km}\,\text{day}^{-1}$ in CFSR and $-39\,\text{km}\,\text{day}^{-1}$ in HiFLOR) compared to NA TCs (mean $-27\,\text{km}\,\text{day}^{-1}$ in CFSR and $-23\,\text{km}\,\text{day}^{-1}$ in HiFLOR). In both basins, these rates of r_8 decay are smaller in magnitude than growth rates of r_8 that occur prior to lifetime maximum r_8. WNP TCs also exhibit a longer duration of r_8 decreases than NA TCs in both the CFSR and HiFLOR.

Finer time-scale variability is also provided by examining the distribution of dr_8/dt (1-day rate of r_8 change) during the end of the TC lifetime (Fig. 6). On this short time scale, the vast majority of dr_8/dt values are negative in both the NA and WNP for CFSR and HiFLOR TCs. Compared to the NA, values of dr_8/dt for WNP TCs are shifted toward more negative values.

These results suggest that WNP TCs exhibit decreases in r_8 that are both larger in magnitude and longer lived than their NA counterparts following lifetime maximum r_8. In the NA, these decreases in r_8 occur near the last few days of the TC lifetime as shown in the representative case studies discussed earlier (Fig. 1a) but not in the composited lifetime plots of r_8 (Figs. 2a,b) because of the relatively large temporal bin width used. These interbasin differences in end-of-lifetime r_8 decreases may reflect stronger, lower-latitude meridional gradients of potential intensity and its component variables in the WNP (e.g., Emanuel 1986, 1987; Chavas and Emanuel 2014), which have been linked to outer size changes. Further differences in the environmental forcing for r_8 may be demonstrated by the stronger baroclinic growth rate and its

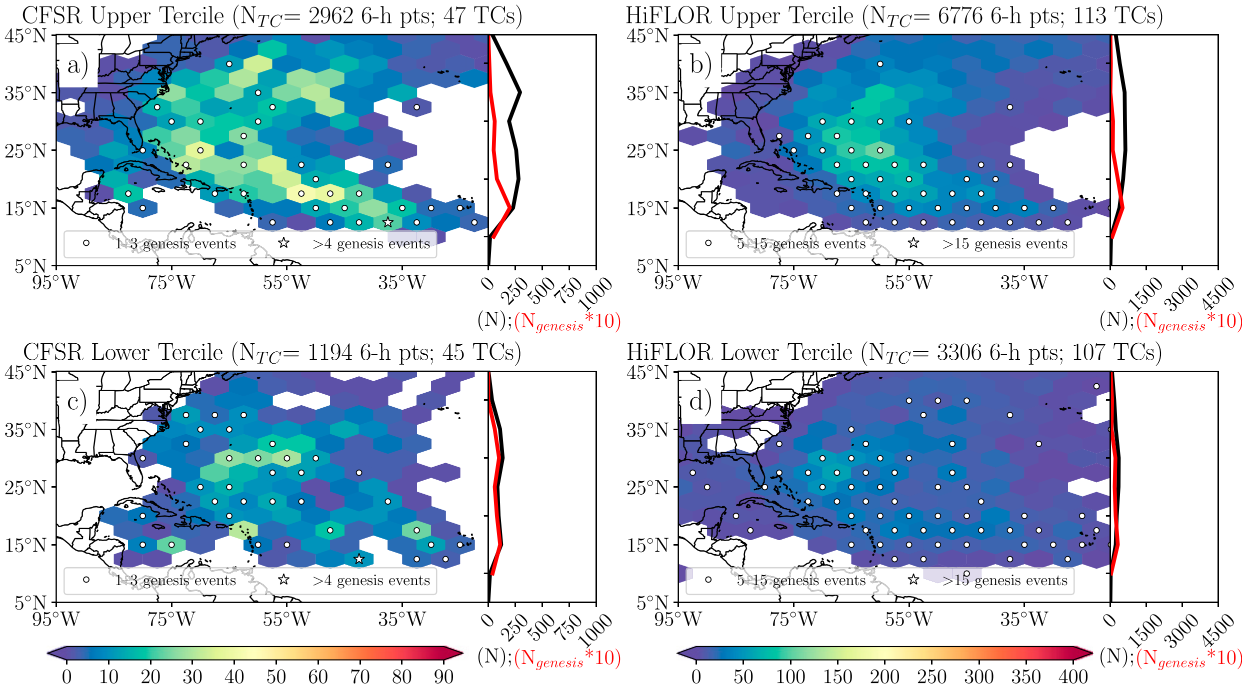

FIG. 8. Plan view plot of number of 6-h TC data points (N; shaded hexagons) and genesis locations (N_{genesis}; white dots and stars) for a ~5.0° latitude × ~5.0° longitude hexagonal grid and zonal sum of the track count (N; solid black line) and genesis location count ($N \times 10$; solid red line; right panel) for TCs within the upper tercile of the r_8 growth between genesis r_8 and lifetime maximum r_8 from the (a) NA CFSR and (b) NA HiFLOR and the lower tercile for the (c) NA CFSR and (d) NA HiFLOR.

larger meridional gradient at equatorward latitudes in the WNP (e.g., Hart and Evans 2001; Kitabatake 2011). Last, the longer duration of r_8 decreases in the WNP may be partially reflective of their larger lifetime maximum outer size compared to the NA, which may result in longer dissipation times upon reaching an unfavorable environment for intensification (e.g., Chen et al. 2011; Carrasco et al. 2014).

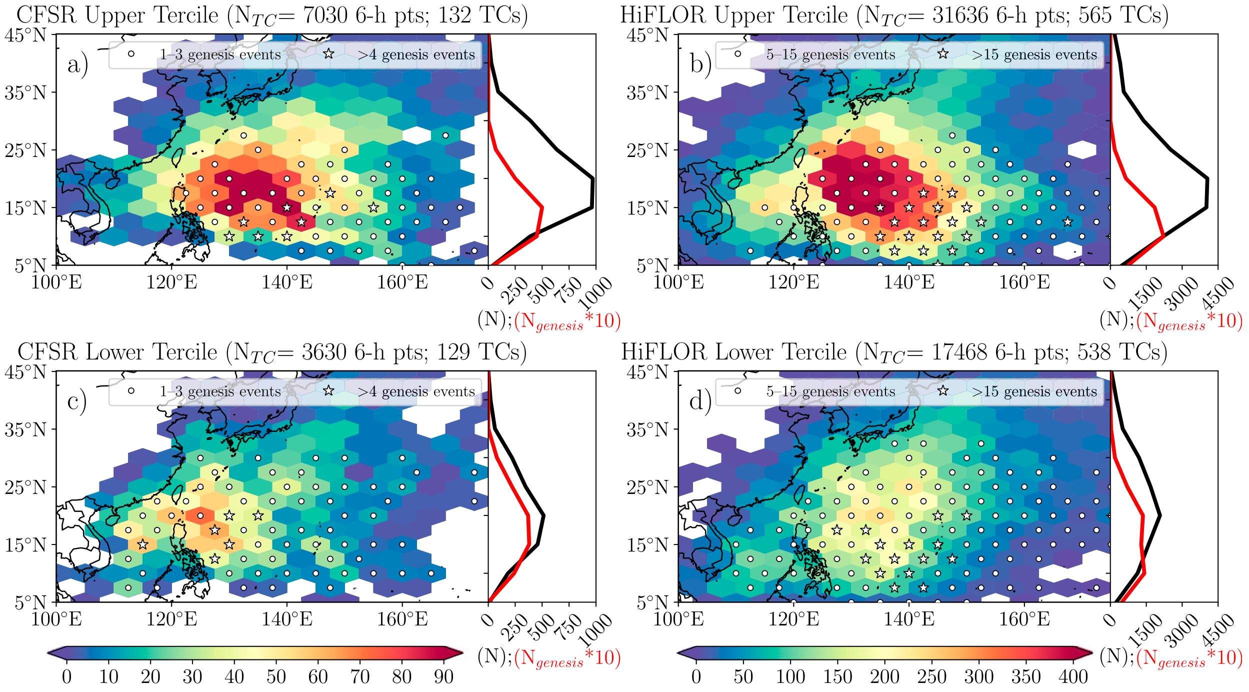

FIG. 9. As in Fig. 8, but for WNP TCs.

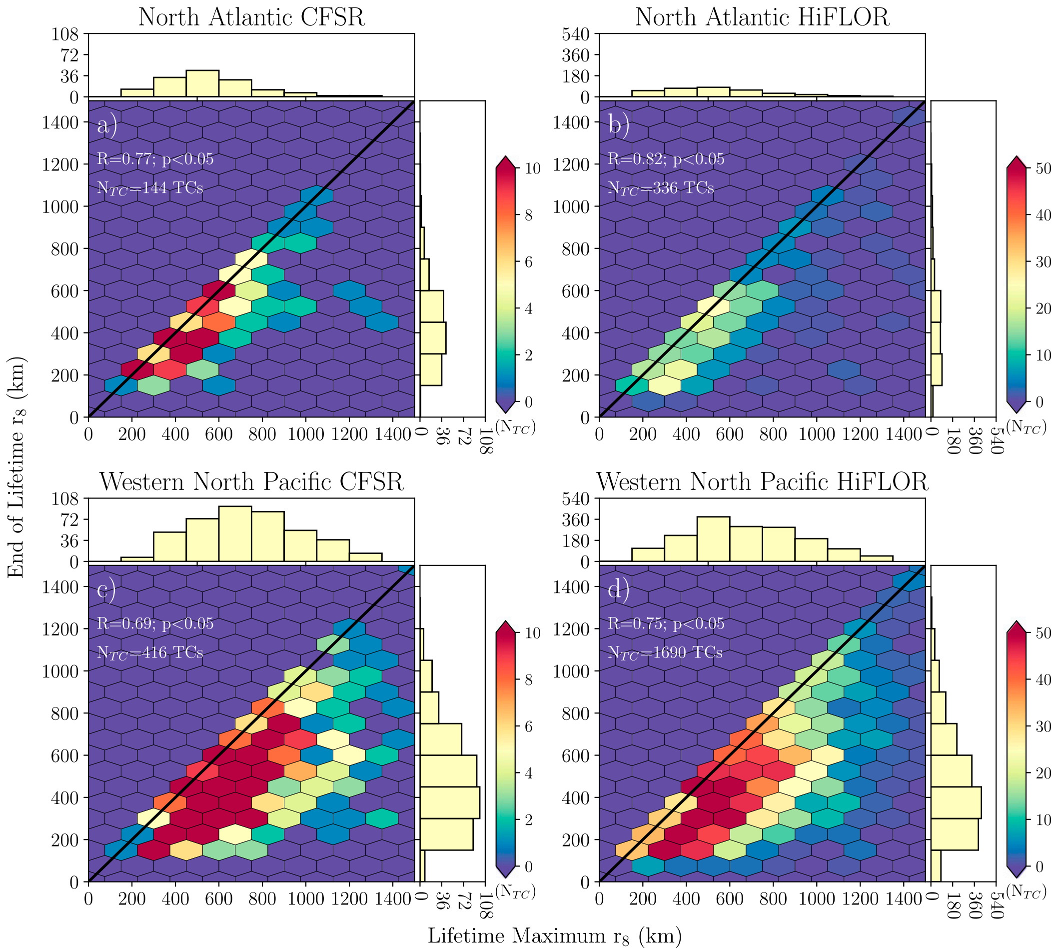

FIG. 10. As in Fig. 3, but for lifetime maximum r_8 (km) vs end-of-lifetime r_8 (km).

d. *Outer TC size evolution during ET*

The final results section examines r_8 changes during ET, starting with joint histograms of r_8 during the day prior to ET versus centered on the end of ET for NA (Figs. 13a,b) and WNP TCs (Figs. 13c,d). In the NA, both the CFSR and HiFLOR show negligible changes in r_8 during ET, while disagreement exists regarding WNP r_8 evolution between the CFSR (small decreases in r_8 during ET) and HiFLOR (no change). The absence of r_8 changes during ET in the NA and, to a lesser degree, the WNP may be partially attributable to the short duration of ET in both the NA (median of 1 day in CFSR and 1.50 days in HiFLOR) and WNP (median of 1.50 days in CFSR and 1.25 days in HiFLOR), consistent with prior work (e.g., Evans and Hart 2003; Kitabatake 2011), coupled with the slow response of the outer wind field to environmental forcing (e.g., Weatherford and Gray 1988; Merrill 1984; Chavas and Emanuel 2010; Chavas and Lin 2016). Both the CFSR and HiFLOR show that WNP TCs are larger than NA TCs prior to ET onset.

Radial profiles of the azimuthal-mean 10-m azimuthal wind in normalized coordinates are provided prior to the start and at the end of ET for NA (Figs. 14a,b) and WNP TCs (Figs. 14c,d). NA TCs exhibit marginal increases in azimuthal winds during ET at outer radii [r/(pre-ET r_8) > 0.75] in both the CFSR and HiFLOR, although these increases in azimuthal winds are not associated with statistically meaningful changes in r_8 for NA ET cases in either the CFSR or HiFLOR. Consistent with the r_8 results for WNP TCs, the CFSR shows decreased azimuthal winds at almost all radii [r/(pre-ET r_8) > 0.2], while HiFLOR shows little change in outer azimuthal winds [r/(pre-ET r_8) > 0.5].

Together, these results show that NA TCs exhibit little change in outer structure during ET, while WNP TCs either exhibit a spindown of the TC wind field or no change, depending on the dataset examined. These results disagree with prior assertions that outer size increases for most TCs during ET (e.g., Brand and Guard 1979; Hart et al. 2006; Evans and Hart 2008), although

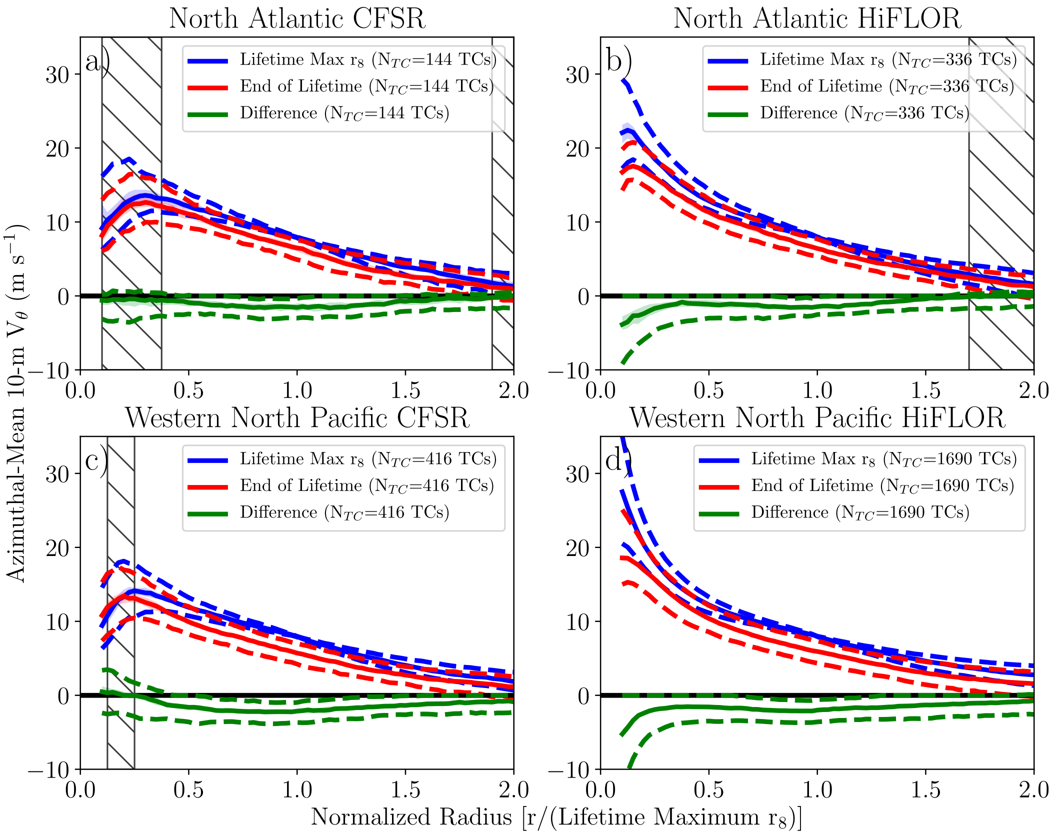

FIG. 11. As in Fig. 4, but during lifetime maximum r_8, end of lifetime, and the difference between the two (m s^{-1}) in a normalized radial coordinate system defined with respect to lifetime maximum r_8 [r/(lifetime maximum r_8)]. The hatching denotes radii at which the distribution of ET start and end values at each radius are likely similar according to two-sample Kolmogorov–Smirnov testing ($p \geq 0.05$).

these prior studies contain uncertainties associated with the absence of statistical testing and small ET sample sizes. Indeed, only a small fraction of cases exhibit their peak r_8 during ET in the NA (17% in CFSR and 33% in HiFLOR) and WNP (5% in CFSR and 10% in HiFLOR). Also, for NA TCs, neither r_8 nor its rate of change for ET cases is larger relative to non-ET cases at the end of their lifetimes for both the CFSR and HiFLOR. WNP ET and non-ET TCs, however, show differing results between the CFSR and HiFLOR, with the CFSR showing no differences between ET and non-ET storms and HiFLOR suggesting that ET r_8 is larger and its rate of change is less likely to be negative at the end of their lifetimes compared to non-ET cases. The lack of r_8 growth during ET may be due to outer TC size at ET start being comparable, or even larger (e.g., WNP CFSR TCs), than extratropical cyclone outer size (e.g., Nielsen and Dole 1992; Simmonds 2000; Rudeva and Gulev 2007) or that statistically meaningful changes in r_8 only begin to occur following the ET end (e.g., Brand and Guard 1979; Hart et al. 2006; Evans and Hart 2008). The absence of increases in r_8 during ET may not be surprising given that the Rossby radius of deformation should decrease during ET (assuming poleward TC motion) because of increases in planetary vorticity, decreases in the depth of the troposphere, and the spindown of the inner-core circulation of the TC (e.g., Hart and Evans 2001; Jones et al. 2003; Hart et al. 2006). The absence of increases in r_8 during ET may suggest that the structural changes that occur during ET (e.g., development of warm conveyor belt; Evans and Hart 2008) are no more efficient at importing angular momentum and spinning up the outer TC circulation than the secondary circulation of the TC (e.g., Merrill 1984; Smith et al. 2011; Chavas and Emanuel 2014).

4. Summary and discussion

The present study examines the lifetime evolution of outer TC size (r_8) and structure for NA and WNP TCs using reanalysis data (CFSR) to represent IBTrACS

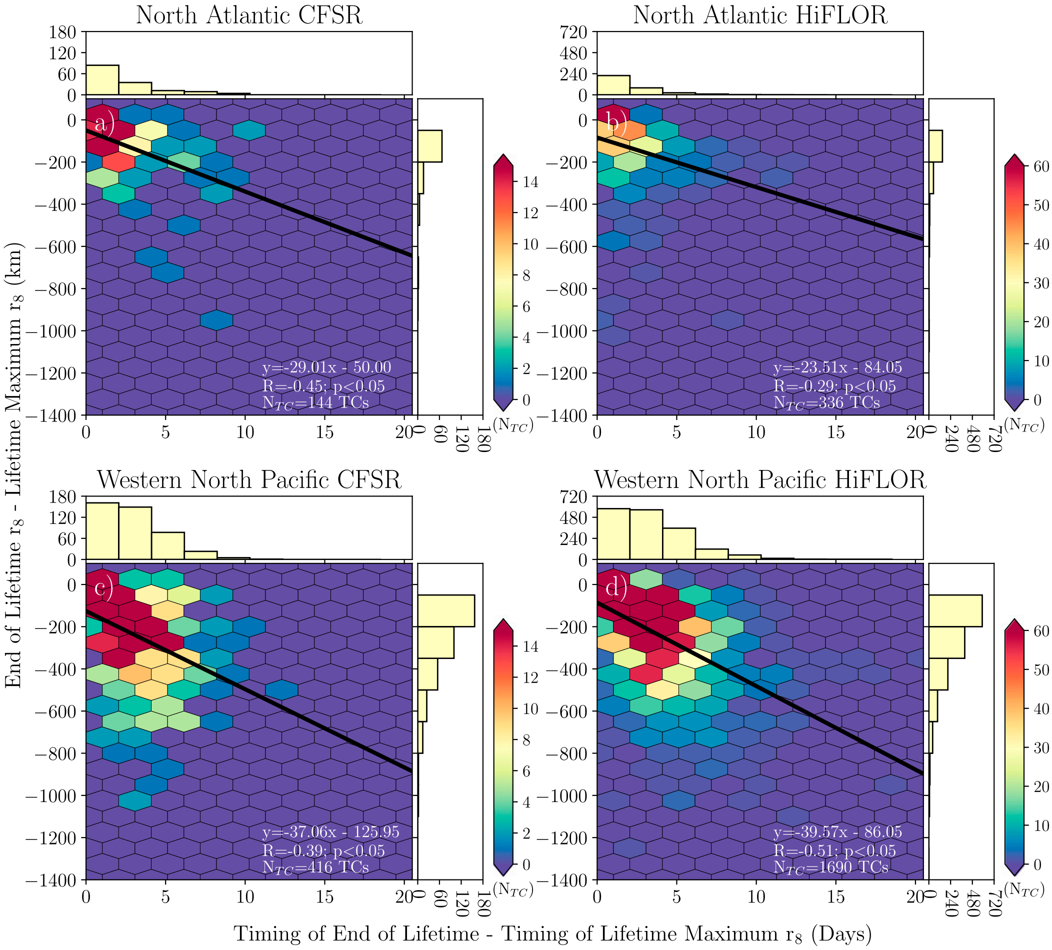

FIG. 12. As in Fig. 3, but for difference between onset of end of lifetime and lifetime maximum r_8 (days) vs the difference between end-of-lifetime r_8 and lifetime maximum r_8 (km). The black solid line denotes the simple linear regression equation between the two quantities with the corresponding equation given in each joint histogram.

TCs and high-resolution climate model data (HiFLOR). The analysis examines representative case studies followed by the composite lifetime evolution of r_8. The interstorm variability of r_8 and outer structure is also examined during three milestones of TC lifetime: genesis, the onset of lifetime maximum r_8, and end of lifetime. Specific focus is placed on examining the time scales of these r_8 changes and their association with certain TC track types as proxies for environmental factors. Finally, we examine the evolution of the outer TC wind field during ET.

We find that r_8 substantially increases throughout most of the TC lifetime for the majority of NA TCs. In comparison, WNP TCs exhibit greater r_8 growth rates, an earlier lifetime peak in r_8, and larger decreases in r_8 at the end of the TC lifetime. In both basins, TCs with short lifetimes exhibit marginal or negligible changes in r_8. These results contrast with prior work suggesting small increases in outer size (Merrill 1984; Chavas and Emanuel 2010) or increases in outer size throughout the entire TC lifetime (Cocks and Gray 2002). Compared to the NA, WNP TCs are systematically larger until the end of their lifetimes.

More specifically, increases in r_8 following genesis in both basins are symptomatic of an expansion of the TC wind field. TCs with a later onset of their peak r_8 tend to be larger TCs. The longest-lived TCs in both basins, especially those recurving TCs, also exhibit the largest growth in r_8. These results may suggest some inherent predictability of r_8 given the large-scale environmental controls on TC genesis and track features.

The decrease in r_8 following lifetime maximum r_8 in both the NA and WNP is associated with the contraction of the outer TC wind field. In addition to exhibiting more rapid decreases in r_8 compared to the NA, these declines occur over a longer duration in the WNP. While genesis outer size imparts some memory upon

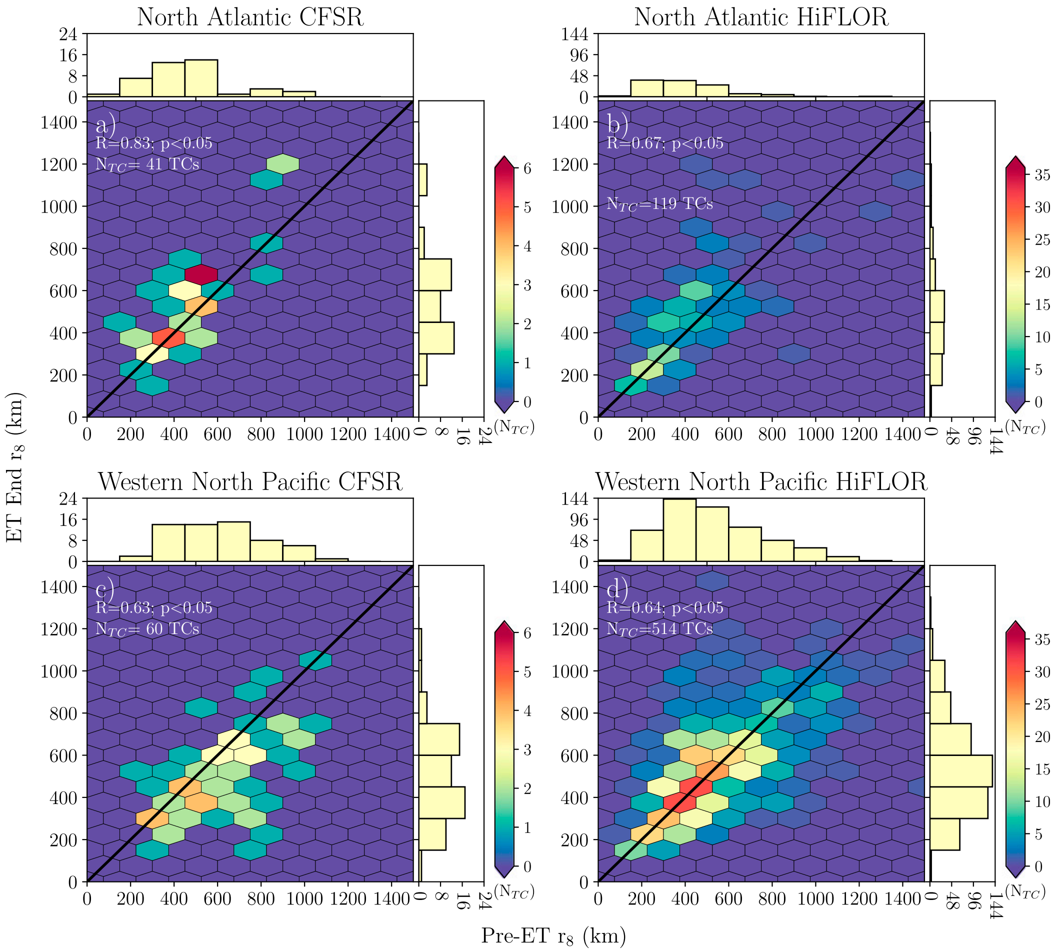

FIG. 13. As in Fig. 3, but for r_8 (km) averaged during the day prior to ET start (km) vs during the day centered on ET end (km).

outer size during the early parts of the TC lifetime, it has relatively little bearing on the end-of-lifetime outer size, which disagrees with previous studies (e.g., Rotunno and Emanuel 1987; Cocks and Gray 2002; Lee et al. 2010).

Finally, we have shown that ET is not associated with substantial changes in r_8 in the NA, while WNP ET cases either exhibit decreases or negligible changes in r_8. These results contrast with the increases in outer size during ET noted in prior work (e.g., Brand and Guard 1979; Hart et al. 2006; Evans and Hart 2008). The absence of outer size changes during ET suggests that the ET processes are no more efficient at broadening the outer TC wind field than purely tropical processes.

Together, these results provide one of the first comprehensive analyses of the lifetime evolution of r_8 and its variability within and among basins. The strong agreement between the two independent datasets used in this study instills greater confidence in our results compared to examining each dataset in isolation from one another and suggests that their respective biases do not impact our results. However, the environmental factors that influence the lifetime variability of outer size remain unclear. The more rapid changes in outer size along with the earlier lifetime peak at lower latitudes in the WNP compared to the NA (e.g., Chan and Chan 2012, 2015; Chavas and Lin 2016) may reflect interbasin differences in their large-scale environment. Moreover, the variability in the lifetime evolution of outer size may be reflective of several environmental factors simultaneously influencing outer size (e.g., angular momentum, relative humidity; Merrill 1984; Hill and Lackmann 2009; Chan and Chan 2013), similar to the evolution of TC intensity (e.g., SSTs, vertical wind shear; Emanuel 1986; Tang and Emanuel 2010; Lin et al. 2017). Ongoing work is leveraging these results to address these outstanding issues.

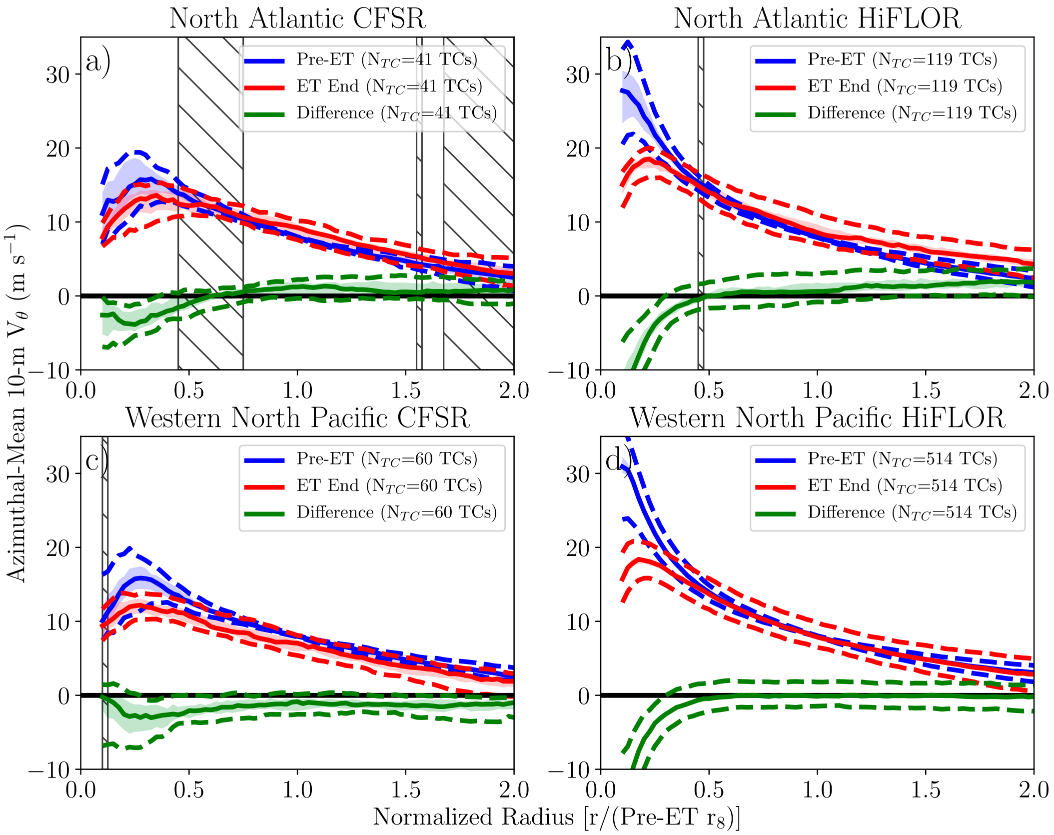

FIG. 14. As in Fig. 4, but at day prior to ET start (pre-ET), at ET end, and the difference between the two (m s^{-1}) in a normalized radial coordinate system defined with respect to r_8 prior to ET start [r/(pre-ET r_8)]. The hatching denotes radii at which the distribution of pre-ET and ET end values at each radius are likely similar according to two-sample Kolmogorov–Smirnov testing ($p \geq 0.05$).

Acknowledgments. This study is supported by EAR-1520683 from NSF and NA15NWS4680005 and NA14OAR4830101 from NOAA. The statements, findings, conclusions, and recommendations herein are those of the authors and do not necessarily reflect the views of NSF and NOAA. This research has bentefited from constructive input from three anonymous reviewers, Hiroyuki Murakami (NOAA/GFDL), Maofeng Liu (Princeton), Clark Evans (UWM), and Sharon Sessions (NMT). This work would not have been possible without the availability of the CFSR and HiFLOR from NCEP and GFDL, respectively. All computations were done in Python, and figures were made using Matplotlib (Hunter 2007).

REFERENCES

Bosilovich, M. G., J. Kennedy, D. Dee, R. Allan, and A. O'Neill, 2013: On the reprocessing and reanalysis of observations for climate. *Climate Science for Serving Society: Research, Modeling and Prediction Priorities*, A. Ghassem and J. W. Hurrell, Eds., Springer, 51–71.

Brammer, A., 2017: Tropical cyclone vortex tracker. Zenodo, https://doi.org/10.5281/zenodo.266194.

Brand, S., and C. P. Guard, 1979: An observational study of extratropical storms evolved from tropical cyclones in the western North Pacific. *J. Meteor. Soc. Japan*, **57**, 479–483, https://doi.org/10.2151/jmsj1965.57.5_479.

Burpee, R. W., 1974: Characteristics of North African easterly waves during the summers of 1968 and 1969. *J. Atmos. Sci.*, **31**, 1556–1570, https://doi.org/10.1175/1520-0469(1974)031<1556:CONAEW>2.0.CO;2.

Camargo, S. J., and A. H. Sobel, 2005: Western North Pacific tropical cyclone intensity and ENSO. *J. Climate*, **18**, 2996–3006, https://doi.org/10.1175/JCLI3457.1.

Carrasco, C. A., C. W. Landsea, and Y.-L. Lin, 2014: The influence of tropical cyclone size on its intensification. *Wea. Forecasting*, **29**, 582–590, https://doi.org/10.1175/WAF-D-13-00092.1.

Chan, K. T. F., and J. C. L. Chan, 2012: Size and strength of tropical cyclones as inferred from QuikSCAT data. *Mon. Wea. Rev.*, **140**, 811–824, https://doi.org/10.1175/MWR-D-10-05062.1.

——, and ——, 2013: Angular momentum transports and synoptic flow patterns associated with tropical cyclone size change. *Mon. Wea. Rev.*, **141**, 3985–4007, https://doi.org/10.1175/MWR-D-12-00204.1.

——, and ——, 2014: Impacts of initial vortex size and planetary vorticity on tropical cyclone size. *Quart. J. Roy. Meteor. Soc.*, **140**, 2235–2248, https://doi.org/10.1002/qj.2292.

——, and ——, 2015: Global climatology of tropical cyclone size as inferred from QuikSCAT data. *Int. J. Climatol.*, **35**, 4843–4848, https://doi.org/10.1002/joc.4307.

Chavas, D. R., and K. A. Emanuel, 2010: A QuikSCAT climatology of tropical cyclone size. *Geophys. Res. Lett.*, **37**, L18816, https://doi.org/10.1029/2010GL044558.

——, and ——, 2014: Equilibrium tropical cyclone size in an idealized state of axisymmetric radiative–convective equilibrium. *J. Atmos. Sci.*, **71**, 1663–1680, https://doi.org/10.1175/JAS-D-13-0155.1.

——, and J. Vigh, 2014: QSCAT-R: The QuikSCAT tropical cyclone radial structure dataset. NCAR Tech. Note NCAR/TN-5131STR, 25 pp., https://doi.org/10.5065/D6J67DZ4.

——, and N. Lin, 2016: A model for the complete radial structure of the tropical cyclone wind field. Part II: Wind field variability. *J. Atmos. Sci.*, **73**, 3093–3113, https://doi.org/10.1175/JAS-D-15-0185.1.

——, ——, and K. Emanuel, 2015: A model for the complete radial structure of the tropical cyclone wind field. Part I: Comparison with observed structure. *J. Atmos. Sci.*, **72**, 3647–3662, https://doi.org/10.1175/JAS-D-15-0014.1.

——, ——, W. Dong, and Y. Lin, 2016: Observed tropical cyclone size revisited. *J. Climate*, **29**, 2923–2939, https://doi.org/10.1175/JCLI-D-15-0731.1.

——, K. A. Reed, and J. A. Knaff, 2017: Physical understanding of the tropical cyclone wind-pressure relationship. *Nat. Commun.*, **8**, 1360, https://doi.org/10.1038/s41467-017-01546-9.

Chen, D. Y.-C., K. K. W. Cheung, and C.-S. Lee, 2011: Some implications of core regime wind structures in western North Pacific tropical cyclones. *Wea. Forecasting*, **26**, 61–75, https://doi.org/10.1175/2010WAF2222420.1.

Cocks, S. B., and W. M. Gray, 2002: Variability of the outer wind profiles of western North Pacific typhoons: Classifications and techniques for analysis and forecasting. *Mon. Wea. Rev.*, **130**, 1989–2005, https://doi.org/10.1175/1520-0493(2002)130<1989:VOTOWP>2.0.CO;2.

Colbert, A. J., and B. J. Soden, 2012: Climatological variations in North Atlantic tropical cyclone tracks. *J. Climate*, **25**, 657–673, https://doi.org/10.1175/JCLI-D-11-00034.1.

Diaz, M., and A. Aiyyer, 2013: Energy dispersion in African easterly waves. *J. Atmos. Sci.*, **70**, 130–145, https://doi.org/10.1175/JAS-D-12-019.1.

Dickinson, M., and J. Molinari, 2002: Mixed Rossby–gravity waves and western Pacific tropical cyclogenesis. Part I: Synoptic evolution. *J. Atmos. Sci.*, **59**, 2183–2196, https://doi.org/10.1175/1520-0469(2002)059<2183:MRGWAW>2.0.CO;2.

Emanuel, K. A., 1986: An air–sea interaction theory for tropical cyclones. Part I: Steady-state maintenance. *J. Atmos. Sci.*, **43**, 585–604, https://doi.org/10.1175/1520-0469(1986)043<0585:AASITF>2.0.CO;2.

——, 1987: The dependence of hurricane intensity on climate. *Nature*, **326**, 483–485, https://doi.org/10.1038/326483a0.

——, 2004: Tropical cyclone energetics and structure. *Atmospheric Turbulence and Mesoscale Meteorology*, E. Federovich, R. Rotunno, and B. Stevens, Eds., Cambridge University Press, 165–192.

Evans, C., and R. E. Hart, 2008: Analysis of the wind field evolution associated with the extratropical transition of Bonnie (1998). *Mon. Wea. Rev.*, **136**, 2047–2065, https://doi.org/10.1175/2007MWR2051.1.

Evans, J. L., and R. E. Hart, 2003: Objective indicators of the life cycle evolution of extratropical transition for Atlantic tropical cyclones. *Mon. Wea. Rev.*, **131**, 909–925, https://doi.org/10.1175/1520-0493(2003)131<0909:OIOTLC>2.0.CO;2.

Frank, W. M., and P. E. Roundy, 2006: The role of tropical waves in tropical cyclogenesis. *Mon. Wea. Rev.*, **134**, 2397–2417, https://doi.org/10.1175/MWR3204.1.

Harris, L. M., S.-J. Lin, and C. Tu, 2016: High-resolution climate simulations using GFDL HiRAM with a stretched global grid. *J. Climate*, **29**, 4293–4314, https://doi.org/10.1175/JCLI-D-15-0389.1.

Hart, R. E., 2003: A cyclone phase space derived from thermal wind and thermal asymmetry. *Mon. Wea. Rev.*, **131**, 585–616, https://doi.org/10.1175/1520-0493(2003)131<0585:ACPSDF>2.0.CO;2.

——, and J. L. Evans, 2001: A climatology of the extratropical transition of Atlantic tropical cyclones. *J. Climate*, **14**, 546–564, https://doi.org/10.1175/1520-0442(2001)014<0546:ACOTET>2.0.CO;2.

——, ——, and C. Evans, 2006: Synoptic composites of the extratropical transition life cycle of North Atlantic tropical cyclones: Factors determining posttransition evolution. *Mon. Wea. Rev.*, **134**, 553–578, https://doi.org/10.1175/MWR3082.1.

Held, I. M., and M. Zhao, 2008: Horizontally homogeneous rotating radiative–convective equilibria at GCM resolution. *J. Atmos. Sci.*, **65**, 2003–2013, https://doi.org/10.1175/2007JAS2604.1.

Hill, K. A., and G. M. Lackmann, 2009: Influence of environmental humidity on tropical cyclone size. *Mon. Wea. Rev.*, **137**, 3294–3315, https://doi.org/10.1175/2009MWR2679.1.

Hodges, K., A. Cobb, and P. L. Vidale, 2017: How well are tropical cyclones represented in reanalysis datasets? *J. Climate*, **30**, 5243–5264, https://doi.org/10.1175/JCLI-D-16-0557.1.

Hunter, J. D., 2007: Matplotlib: A 2D graphics environment. *Comput. Sci. Eng.*, **9**, 90–95, https://doi.org/10.1109/MCSE.2007.55.

Jones, S. C., and Coauthors, 2003: The extratropical transition of tropical cyclones: Forecast challenges, current understanding, and future directions. *Wea. Forecasting*, **18**, 1052–1092, https://doi.org/10.1175/1520-0434(2003)018<1052:TETOTC>2.0.CO;2.

Khairoutdinov, M., and K. Emanuel, 2013: Rotating radiative-convective equilibrium simulated by a cloud-resolving model. *J. Adv. Model. Earth Syst.*, **5**, 816–825, https://doi.org/10.1002/2013MS000253.

Kimball, S. K., 2006: A modeling study of hurricane landfall in a dry environment. *Mon. Wea. Rev.*, **134**, 1901–1918, https://doi.org/10.1175/MWR3155.1.

——, and M. S. Mulekar, 2004: A 15-year climatology of North Atlantic tropical cyclones. Part I: Size parameters. *J. Climate*, **17**, 3555–3575, https://doi.org/10.1175/1520-0442(2004)017<3555:AYCONA>2.0.CO;2.

Kitabatake, N., 2011: Climatology of extratropical transition of tropical cyclones in the western North Pacific defined by using cyclone phase space. *J. Meteor. Soc. Japan*, **89**, 309–325, https://doi.org/10.2151/jmsj.2011-402.

Knaff, J. A., S. P. Longmore, and D. A. Molenar, 2014: An objective satellite-based tropical cyclone size climatology. *J. Climate*, **27**, 455–476, https://doi.org/10.1175/JCLI-D-13-00096.1; Corrigendum, **28**, 8648–8651, https://doi.org/10.1175/JCLI-D-15-0610.1.

Knapp, K. R., M. C. Kruk, D. H. Levinson, H. J. Diamond, and C. J. Neumann, 2010: The International Best Track Archive for Climate Stewardship (IBTrACS) unifying tropical cyclone data. *Bull. Amer. Meteor. Soc.*, **91**, 363–376, https://doi.org/10.1175/2009BAMS2755.1.

Kossin, J. P., K. R. Knapp, D. J. Vimont, R. J. Murnane, and B. A. Harper, 2007: A globally consistent reanalysis of hurricane variability and trends. *Geophys. Res. Lett.*, **34**, L04815, https://doi.org/10.1029/2006GL028836.

——, S. J. Camargo, and M. Sitkowski, 2010: Climate modulation of North Atlantic hurricane tracks. *J. Climate*, **23**, 3057–3076, https://doi.org/10.1175/2010JCLI3497.1.

Lander, M. A., 1994: Description of a monsoon gyre and its effects on the tropical cyclones in the western North Pacific during August 1991. *Wea. Forecasting*, **9**, 640–654, https://doi.org/10.1175/1520-0434(1994)009<0640:DOAMGA>2.0.CO;2.

Landsea, C. W., B. A. Harper, K. Hoarau, and J. A. Knaff, 2006: Can we detect trends in extreme tropical cyclones? *Science*, **313**, 452–454, https://doi.org/10.1126/science.1128448.

Lee, C.-S., K. K. W. Cheung, W.-T. Fang, and R. L. Elsberry, 2010: Initial maintenance of tropical cyclone size in the western North Pacific. *Mon. Wea. Rev.*, **138**, 3207–3223, https://doi.org/10.1175/2010MWR3023.1.

Lin, N., and D. Chavas, 2012: On hurricane parametric wind and applications in storm surge modeling. *J. Geophys. Res.*, **117**, D09120, https://doi.org/10.1029/2011JD017126.

——, R. Jing, Y. Wang, E. Yonekura, J. Fan, and L. Xue, 2017: A statistical investigation of the dependence of tropical cyclone intensity change on the surrounding environment. *Mon. Wea. Rev.*, **145**, 2813–2831, https://doi.org/10.1175/MWR-D-16-0368.1.

Liu, K. S., and J. C. L. Chan, 1999: Size of tropical cyclones as inferred from *ERS-1* and *ERS-2* data. *Mon. Wea. Rev.*, **127**, 2992–3001, https://doi.org/10.1175/1520-0493(1999)127<2992:SOTCAI>2.0.CO;2.

Liu, M., G. A. Vecchi, J. A. Smith, and H. Murakami, 2017: The present-day simulation and twenty-first-century projection of the climatology of extratropical transition in the North Atlantic. *J. Climate*, **30**, 2739–2756, https://doi.org/10.1175/JCLI-D-16-0352.1.

Loridan, T., E. Scherer, M. Dixon, E. Bellone, and S. Khare, 2014: Cyclone wind field asymmetries during extratropical transition in the western North Pacific. *J. Appl. Meteor. Climatol.*, **53**, 421–428, https://doi.org/10.1175/JAMC-D-13-0257.1.

——, S. Khare, E. Scherer, M. Dixon, and E. Bellone, 2015: Parametric modeling of transitioning cyclone wind fields for risk assessment studies in the western North Pacific. *J. Appl. Meteor. Climatol.*, **54**, 624–642, https://doi.org/10.1175/JAMC-D-14-0095.1.

Maclay, K. S., M. DeMaria, and T. H. Vonder Haar, 2008: Tropical cyclone inner-core kinetic energy evolution. *Mon. Wea. Rev.*, **136**, 4882–4898, https://doi.org/10.1175/2008MWR2268.1.

Manning, D. M., and R. E. Hart, 2007: Evolution of North Atlantic ERA40 tropical cyclone representation. *Geophys. Res. Lett.*, **34**, L05705, https://doi.org/10.1029/2006GL028266.

Marchok, T. P., 2002: How the NCEP tropical cyclone tracker works. *25th Conf. on Hurricanes and Tropical Meteorology*, San Diego, CA, Amer. Meteor. Soc., P1.13, https://ams.confex.com/ams/pdfpapers/37628.pdf.

Merrill, R. T., 1984: A comparison of large and small tropical cyclones. *Mon. Wea. Rev.*, **112**, 1408–1418, https://doi.org/10.1175/1520-0493(1984)112<1408:ACOLAS>2.0.CO;2.

Murakami, H., 2014: Tropical cyclones in reanalysis data sets. *Geophys. Res. Lett.*, **41**, 2133–2141, https://doi.org/10.1002/2014GL059519.

——, and Coauthors, 2015: Simulation and prediction of category 4 and 5 hurricanes in the high-resolution GFDL HiFLOR coupled climate model. *J. Climate*, **28**, 9058–9079, https://doi.org/10.1175/JCLI-D-15-0216.1.

——, and Coauthors, 2016: Seasonal forecasts of major hurricanes and landfalling tropical cyclones using a high-resolution GFDL coupled climate model. *J. Climate*, **29**, 7977–7989, https://doi.org/10.1175/JCLI-D-16-0233.1.

Nielsen, J. W., and R. M. Dole, 1992: A survey of extratropical cyclone characteristics during GALE. *Mon. Wea. Rev.*, **120**, 1156–1168, https://doi.org/10.1175/1520-0493(1992)120<1156:ASOECC>2.0.CO;2.

Parker, W. S., 2016: Reanalyses and observations: What's the difference? *Bull. Amer. Meteor. Soc.*, **97**, 1565–1572, https://doi.org/10.1175/BAMS-D-14-00226.1.

Rayner, N. A., D. E. Parker, E. B. Horton, C. K. Folland, L. V. Alexander, D. P. Rowell, E. C. Kent, and A. Kaplan, 2003: Global analyses of sea surface temperature, sea ice, and night marine air temperature since the late nineteenth century. *J. Geophys. Res.*, **108**, 4407, https://doi.org/10.1029/2002JD002670.

Reed, R. J., D. C. Norquist, and E. E. Recker, 1977: The structure and properties of African wave disturbances as observed during phase III of GATE. *Mon. Wea. Rev.*, **105**, 317–333, https://doi.org/10.1175/1520-0493(1977)105<0317:TSAPOA>2.0.CO;2.

Rotunno, R., and K. A. Emanuel, 1987: An air–sea interaction theory for tropical cyclones. Part II: Evolutionary study using a nonhydrostatic axisymmetric numerical model. *J. Atmos. Sci.*, **44**, 542–561, https://doi.org/10.1175/1520-0469(1987)044<0542:AAITFT>2.0.CO;2.

Rudeva, I., and S. K. Gulev, 2007: Climatology of cyclone size characteristics and their changes during the cyclone life cycle. *Mon. Wea. Rev.*, **135**, 2568–2587, https://doi.org/10.1175/MWR3420.1.

Saha, S., and Coauthors, 2010: The NCEP Climate Forecast System Reanalysis. *Bull. Amer. Meteor. Soc.*, **91**, 1015–1057, https://doi.org/10.1175/2010BAMS3001.1.

Schenkel, B. A., and R. E. Hart, 2012: An examination of tropical cyclone position, intensity, and intensity life cycle within atmospheric reanalysis datasets. *J. Climate*, **25**, 3453–3475, https://doi.org/10.1175/2011JCLI4208.1.

——, N. Lin, D. Chavas, M. Oppenheimer, and A. Brammer, 2017: Evaluating outer tropical cyclone size in reanalysis datasets using QuikSCAT data. *J. Climate*, **30**, 8745–8762, https://doi.org/10.1175/JCLI-D-17-0122.1.

Simmonds, I., 2000: Size changes over the life of sea level cyclones in the NCEP reanalysis. *Mon. Wea. Rev.*, **128**, 4118–4125, https://doi.org/10.1175/1520-0493(2000)129<4118:SCOTLO>2.0.CO;2.

Smith, R. K., M. T. Montgomery, and N. V. Sang, 2009: Tropical cyclone spin-up revisited. *Quart. J. Roy. Meteor. Soc.*, **135**, 1321–1335, https://doi.org/10.1002/qj.428.

——, C. W. Schmidt, and M. T. Montgomery, 2011: An investigation of rotational influences on tropical-cyclone size and intensity. *Quart. J. Roy. Meteor. Soc.*, **137**, 1841–1855, https://doi.org/10.1002/qj.862.

Tang, B., and K. Emanuel, 2010: Midlevel ventilation's constraint on tropical cyclone intensity. *J. Atmos. Sci.*, **67**, 1817–1830, https://doi.org/10.1175/2010JAS3318.1.

Thorne, P. W., and R. S. Vose, 2010: Reanalyses suitable for characterizing long-term trends. *Bull. Amer. Meteor. Soc.*, **91**, 353–361, https://doi.org/10.1175/2009BAMS2858.1.

Wang, Y., 2009: How do outer spiral rainbands affect tropical cyclone structure and intensity? *J. Atmos. Sci.*, **66**, 1250–1273, https://doi.org/10.1175/2008JAS2737.1.

Weatherford, C. L., and W. M. Gray, 1988: Typhoon structure as revealed by aircraft reconnaissance. Part I: Data analysis and climatology. *Mon. Wea. Rev.*, **116**, 1032–1043, https://doi.org/10.1175/1520-0493(1988)116<1032:TSARBA>2.0.CO;2.

Wood, K. M., and E. A. Ritchie, 2014: A 40-year climatology of extratropical transition in the eastern North Pacific. *J. Climate*, **27**, 5999–6015, https://doi.org/10.1175/JCLI-D-13-00645.1.